CENTENNIAL-SCALE SEA SURFACE TEMPERATURE AND SALINITY VARIABILITY IN THE FLORIDA STRAITS DURING THE EARLY HOLOCENE

A Thesis

by

WILLIAM ADAM WEINLEIN

Submitted to the Office of Graduate Studies of
Texas A&M University
in partial fulfillment of the requirements for the degree of

MASTER OF SCIENCE

August 2011

Major Subject: Oceanography

CENTENNIAL-SCALE SEA SURFACE TEMPERATURE AND SALINITY VARIABILITY IN THE FLORIDA STRAITS DURING THE EARLY HOLOCENE

A Thesis

by

WILLIAM ADAM WEINLEIN

Submitted to the Office of Graduate Studies of
Texas A&M University
in partial fulfillment of the requirements for the degree of

MASTER OF SCIENCE

Approved by:

Chair of Committee,	Matthew Schmidt
Committee Members,	Mitch Lyle
	Franco Marcantonio
Head of Department,	Piers Chapman

August 2011

Major Subject: Oceanography

ABSTRACT

Centennial-Scale Sea Surface Temperature and Salinity Variability in the Florida Straits During the Early Holocene. (August 2011)

William Adam Weinlein, B.S., Rutgers, the State University of New Jersey

Chair of Advisory Committee: Dr. Matthew Schmidt

Previous studies showed that sea surface salinity (SSS) in the Florida Straits as well as Florida Current transport covaried with changes in North Atlantic climate over the past two millennia. However, little is known about earlier Holocene variability in the Florida Straits. Here, we combine Mg/Ca-paleothermometry and stable oxygen isotope measurements on the planktonic foraminifera *Globigerinoides ruber* (white variety) from Florida Straits sediment core KNR166-2 JPC 51 (24° 24.70' N, 83° 13.14'W, 198m deep) to reconstruct a high-resolution (~30 yr/sample) early to mid Holocene record of sea surface temperature and $\delta^{18}O_{SW}$ (a proxy for SSS) variability. We also measured Ba/Ca ratios in the same shell material as a proxy for riverine input into the Gulf of Mexico over the same time interval. After removing the influence of global $\delta^{18}O_{SW}$ change due to continental ice volume variability, we propose that early Holocene SSS enrichments were caused by increased evaporation/precipitation ratios in the Florida Straits associated with periods of reduced solar output, increased ice rafted debris in the North Atlantic and the development of more permanent El Niño-like conditions in the eastern equatorial Pacific. When considered with previous high-resolution

reconstructions of early Holocene tropical atmospheric circulation changes, our results provide evidence that solar output variability over the Holocene had a significant impact on the global tropical hydrologic cycle over the last 10,000 years.

ACKNOWLEDGEMENTS

I thank my thesis advisor, Dr. Matthew Schmidt, and committee members, Drs. Mitch Lyle and Franco Marcantonio, for their significant contributions to my development and progress in pursuit of my thesis. I also thank Amy Gondran for her assistance with sample collection, Tammy Chang for sample processing, as well as Jennifer Hertzberg, Kelly Cole, Stuart Pearce, and Christopher Paul for statistical analysis. I appreciate the support and advice from friends, family, colleagues, and coworkers for any contribution large or small to my success at Texas A&M University, especially my loving fiancé, Nicole Davidson.

TABLE OF CONTENTS

LIST OF FIGURES

LIST OF TABLES

1. INTRODUCTION

In order to predict how climate will change over the next few centuries, there is a critical need to understand the mechanisms involved in climate dynamics over the current interglacial period, the Holocene. It has been established that the North Atlantic has experienced a number of quasi-periodic climate cycles, the most recent being the Little Ice Age (LIA) from ~150 to 450 yrs BP and the Medieval Warm Period (MWP) from ~700 to 1500 yr BP [*Bond et al.*, 2001; *Poore et al.,* 2003; *Poore et al.*, 2004, *Richey et al.,* 2009; *Keigwin,* 1996; *DeMenocal et al.* 2000]. Nevertheless, very little is known about sub millennial-scale climate oscillations during earlier parts of the Holocene. In addition, the driver of these Holocene climate oscillations is still unknown. While some researchers argue that external forcing (solar variability) is responsible for Holocene climate cycles, others argue for an internal mechanism [*Cane and Clement*, 1999; *Clement and Cane*, 1999]

The Florida Current makes up a major component of the northward flowing Gulf Stream system, and thus forms an important link between the tropics and the high latitude North Atlantic. *Lund and Curry* [2004 and 2006] showed that climate variability in the Florida Straits is linked to high-latitude climate change and *Lund et al.* [2006] found that Florida Current transport is tightly coupled to changes in North Atlantic Meridional Overturning Circulation (AMOC) variability over the past two

---

This thesis follows the style of *Paleoceanography.*

millennia. In particular, the period of reduced AMOC and cooler climate in the North Atlantic during the LIA was associated with drier conditions in the Florida Straits as the Hadley circulation cells and the Intertropical Convergence Zone (ITCZ) shifted southward out of the Caribbean.

In order to determine if the Florida Straits experienced centennial-scale climate oscillations earlier in the Holocene, we generated a high-resolution record of early Holocene sea surface temperature (SST) and sea surface salinity (SSS) variability from a sediment core collected from the Florida Margin of the Florida Straits, KNR166-2 JPC 51 (24° 24.70' N, 83° 13.14'W, 198m deep) (Figure 1). By combining Mg/Ca-paleothermometry and stable oxygen isotope measurements on the planktonic foraminifera *Globigerinodes ruber* (white variety), we reconstruct a high-resolution (~30 yr/sample) early to mid Holocene record from ~9.1 to 6.2 kyr and a lower resolution (~150 yr/sample) mid to late Holocene record from 6.2 to 1.4 kyr (core-top) of $\delta^{18}O_{SW}$ variability in the Florida Straits. After correcting the $\delta^{18}O_{SW}$ record for global changes in $\delta^{18}O_{SW}$ due to continental ice volume variability, the ice volume free $\delta^{18}O_{SW}$ record can be used as a proxy for past changes in SSS. Because *G. ruber* is an abundant planktonic foraminifera that lives in the upper mixed layer, the top several hundred meters [*Bé and Tolderlund*, 1971], it is ideal for reconstructing past changes in surface water conditions. As an additional proxy of SSS variability resulting from riverine input, we also measured Ba/Ca ratios in the same *G. ruber* shell material.

2. OCEANOGRAPHIC SETTING

The Florida Straits are characterized by a high eastward current flow of 31 Sv [*Lund and Curry*, 2006]. Waters from the Caribbean are directly connected with the Florida Straits via flow through the Yucatan Current [*Maul and Vukovich*, 1993; *Murphy et al.,* 1999]. As such, waters in the Florida Straits are predominantly characteristic of the Caribbean [*Brunner,* 1982; *Lynch-Stieglitz et al.,* 2009] and form an important link between waters of the Caribbean, the Gulf of Mexico and North Atlantic (Figure 1).

The climate of the Florida Straits is subtropical in winter and tropical during the summer. The modern seasonal SST cycle in the Florida Straits fluctuates from ~25 to 26°C from January to March then steadily increases to ~29.5°C by August before decreasing to ~26.0°C in December [*Locarnini et al.,* 2006, Figure 2a]. The modern annual average SST is 27.5°C.

Modern annual SSS fluctuates from ~36.1 to 36.2 from January to June, and peaks at ~36.2 in June prior to decreasing to ~35.9 from August to December [*Antonov et. al*, 2006, Figure 2b].

3. METHODS

3.1 Age Model Development

In order to develop an age model for JPC 51, several intervals were sampled for radiocarbon analysis. ^{14}C analyses were conducted using 3.4 to 5.5 mg of *G. ruber* and *G. sacculifer* shells collected from the >355 μm size coarse fraction. These samples were analyzed at the National Ocean Sciences Accelerator Mass Spectrometry Facility of the Woods Hole Oceanographic Institute in Massachusetts. Raw ^{14}C ages were converted to calendar age using CALIB 6.0 (Table 1) [*Stuiver et al.*, 2005]. Linear interpolation between intervals of known ages yields Holocene sedimentation rates in JPC 51 ranging from 60 to 188 cm/kyr (Figure 3).

Our Holocene records span ~7.7 kyr from 9.16 to 1.48 kyr. The upper 295 cm of core JPC 51 corresponds from 6.21 to 1.48 kyr and the lower 254.25 cm corresponds from 9.16 to 6.21 kyr. The age model shows a period of maximum sedimentation rates from 8.0 to 7.3 kyr, when sedimentation rates range from 141 to 188 cm/kyr (Figure 3). Sedimentation rates from 7.3 to 1.4 kyr are relatively constant, ranging from 60 to 83 cm/kyr. In order to develop a high-resolution early Holocene record, we sampled JPC 51 every 2 cm from 554.5 to 300.5 cm and at a lower resolution, every 8 cm, from 296.5 cm to the core top.

3.2 Stable Isotope Analysis

Sediment from each of the 164 intervals was dried overnight at ~50°C, then weighed and disaggregated in ultra clean water for 6 hours on a shaker table. To collect the coarse fraction, samples were wet-sieved using a 63 μm mesh. For each interval, 80

individual *G. ruber* (white variety) specimens were collected from the 255 to 350 μm size fraction. The 255 to 350 μm size fraction limitation was used to minimize ontogenetic and growth rate effects on shell geochemistry [*Lea et al.,* 2000; *Spero et al.,* 2003]. To ensure an unbiased estimation of the average $\delta^{18}O$ value for a given interval, we used 17-25 *G. ruber* shells for individual stable isotope analysis. Samples were sonicated in methanol for 6 seconds then crushed and homogenized prior to analyses. A 100 to 150 μg split of the sample was then analyzed for stable isotopes in J. Lynch-Steiglitz's laboratory at the Georgia Institute of Technology on a Finnigan MAT253 stable isotope ratio mass spectrometer with a Kiel Device. Raw $\delta^{18}O$ values were standardized using NBS-19 and Venato 690 (an in-house standard).

3.3 Minor and Trace Metal Analysis

For minor and trace metal analysis, 45 to 60 *G. ruber* shells (~580 μg) were gently crushed between glass plates under a microscope and then split for duplicate analysis. To maintain trace metal clean conditions, the samples were then cleaned according to the procedures of *Lea et al*. [2000] and *Mashiotta et al.* [1999] in a laminar flow clean bench. The cleaning process included sonication in both ultra clean water and methanol to remove clays, a hot water bath in reducing agents to remove metal oxides and a hot water bath in an oxidizing solution to remove organic matter. Finally, the samples were transferred to acid cleaned vials and leached in weak nitric acid. The samples were analyzed in duplicate on a Thermo Scientific Element XR High Resolution Inductively Coupled Mass Spectrometer (HR-ICP-MS) using isotope dilution, as

outlined in *Lea and Martin* [1996]. A suite of elements including Na, Mg, Ca, Sr, Ba, U, Al, Fe and Mn, were analyzed and reported as metal/Ca ratios.

3.4 Influence of Dissolution and Diagenetic Overprinting on Shell Metal/Ca Ratios and $\delta^{18}O$ Values

When interpreting geochemical proxies in paleoceanographic studies, it is important to quantify the impact of dissolution and reprecipitation of calcium carbonate minerals from sediment pore fluid. Planktonic foraminifera shells can dissolve during descent through the water column and after deposition on the seafloor, causing a reduction in shell Mg/Ca ratios with water depth. Although this effect varies from species to species and between ocean basins [*Brown and Elderfield*, 1996; *Lea et al.*, 2000; *Lorens et al.,* 1977; *Rosenthal and Boyle*, 1993; and *Rosenthal et al*., 2000], the 196 m depth of the core used in this study is well above the lysocline in the Atlantic (modern depth = 5 to 6 km) and is well above the depth where dissolution has been shown to impact foraminiferal Mg/Ca ratios in the Atlantic [*Dekens et al.,* 2002]. In addition, we have not observed any visual evidence of dissolution on the foraminiferal shells we have thus analyzed (i.e. dissolution pits) and the Mg/Ca-based SST estimates from Holocene samples in the cores we use in this study are in good agreement with modern SST measurements.

It is more difficult to identify the presence of Mg-rich mineral precipitates on shell surfaces without additional analyses. To investigate the possibility of diagenetic overprinting by high Mg/Ca overgrowths, several scanning electron microscope images were taken (Figure 4a, b). If present, diagenetic crystal growth appears to be a

crystalline crust that forms on the surface of the shell most often but not limited to filling in pores, gaps and cracks [*Dittert and Henrich*, 2000; *Boussetta et al.* 2011; *van Raden et al.*, 2011]. In contrast, dissolution pits look like dissolved holes in the shell surface. *G. ruber* specimens from intervals in JPC 51 characterized by the highest and lowest Mg/Ca ratios were selected for SEM imaging (Figure 4a, b). Examination of the images shows no evidence of diagenetic crystal growth or dissolution pits on the surface of the shells in either interval. Instead we only see evidence of clays (removed during the cleaning process) on the surface of the shell material and filling the pores. Therefore, it is unlikely that *G. ruber* from JPC 51 is affected by these processes. The images were obtained using a JEOL JSM-6400 with a PGT EDS System at Texas A&M University with the help of Bridget Wade.

3.5 Calculations

Foraminiferal Mg/Ca:temperature relationships have been derived from a combination of experimental, core top, and sediment trap calibrations [*Anand et al.,* 2003; *Dekens et al.,* 2002; *Nurnberg et al.,* 1996]. Because it is unlikely that dissolution is an issue in the shallow core selected for this study, I utilized the non-depth corrected Mg/Ca:SST calibration of *Anand et al.* [2003] to estimate calcification temperatures for the Florida Margin:

$$Mg/Ca = 0.38 \exp(0.09*T) \quad (\text{error } \pm 0.5\ ^{o}C) \qquad \text{(Eq. 1)}$$

This equation was derived from the measurement of Mg/Ca ratios in planktonic foraminifera collected from sediment traps in the Sargasso Sea and modern SST data. The estimated 1σ error on this relationship is between ±0.5 – 1.0 ºC [*Anand et al.,* 2003].

The oxygen isotopic composition of foraminiferal calcite is dependent on the temperature and the ambient isotopic composition of seawater ($\delta^{18}O_{SW}$) in which it precipitates its shell. If the temperature component is accounted for, foraminiferal calcite can be used to estimate past changes in SSS because $\delta^{18}O_{SW}$ covaries linearly with SSS [*Fairbanks et al.,* 1992]. Based on this concept, numerous studies have developed and redefined a multi-proxy geochemical approach in which calibrated Mg/Ca ratios from planktonic foraminifera shells are used to reconstruct past SST [*Elderfield and Ganssen*, 2000; *Hastings et al.,* 1998; *Dekens et al., 2002*; *Mashiotta et al.,* 1999; *Schmidt et al., 2004*]. Subtracting the influence of SST on foraminiferal $\delta^{18}O_C$ results in the calculation of $\delta^{18}O_{SW}$.

Lea et al. [2000] and *Schmidt et al.* [2004] found that the low-light temperature:$\delta^{18}O$ relationship determined for *Orbulina universa* in laboratory culture experiments [*Bemis et al.,* 1998] yields excellent results when applied to fossil *G. ruber* (white variety) to calculate modern $\delta^{18}O_{SW}$ in the equatorial Pacific and Caribbean. Using the *Bemis et al.* [1998] $\delta^{18}O_{calcite}$:SST relationship,

$$(T°C) = 16.5 - 4.80\ (\delta^{18}O_{calcite} - (\delta^{18}O_{seawater} - 0.27‰)) \text{ (error } \pm 0.7\ ºC) \qquad \text{(Eq. 2)}$$

$\delta^{18}O_{calcite}$ values and Mg/Ca SST values were combined to calculate $\delta^{18}O_{seawater}$ ($\delta^{18}O_{SW}$, a proxy for SSS).

3.6 Estimating SSS Change from $\delta^{18}O_{seawater}$

Changes in continental ice volume also affect global $\delta^{18}O_{SW}$ on glacial-interglacial time scales. If this can effect can be accounted for, the resulting ice volume

free $\delta^{18}O_{SW}$ record can be used to estimate regional salinity change. Sea level has risen by ~25 m over the last 10 kyr due to the melting of polar ice sheets [*Bard et al.,* 1990; *Cutler et al.* 2003; *Edwards et al.,* 1993]. Because continental ice is isotopically depleted in $\delta^{18}O$, addition of this meltwater has changed the average global ocean $\delta^{18}O_{SW}$ value by ~0.20‰ over the last 10 kyr. In order to correct for this continental ice volume effect, we used a compilation of sea level records for the last 10 kyr [*Bard et al.,* 1990; *Cutler et al.,* 2003; *Edwards et al.,* 1993]. Using the relationship that a one meter increase in sea level change equates to a change of –0.008‰ in global $\delta^{18}O_{sw}$ values [*Siddall et al.,* 2003], we subtracted global changes in $\delta^{18}O_{sw}$ from our calculated $\delta^{18}O_{sw}$ record, resulting in the regional ice volume free $\delta^{18}O_{sw}$ record, $\delta^{18}O_{IVF\text{-}SW}$.

3.7 Error Analysis

The analytical precision for the $\delta^{18}O$ analyses is less then ±0.07 ‰. The long-term analytical reproducibility of a synthetic, matrix-matched Mg/Ca standard analyzed over the course of this study is ±0.48 % (0.01 stdev), and the pooled standard deviation of my replicate Mg/Ca analyses is ±3.58 % (1 SD, 186 degrees of freedom) based on 164 analyzed intervals. We estimate the error on calculated $\delta^{18}O_{sw}$ values to be ~0.25‰ based on the propagation of the 1 sigma error from the Mg/Ca and $\delta^{18}O$ analyses along with the reported errors from the *Anand et al.* [2003], Equation 1, and the *Bemis et al.* [1998], Equation 2. The long-term analytical reproducibility of our synthetic Ba/Ca standard measured over the course of this study is ±0.50% (0.01 stdev), and the pooled standard deviation on my replicate Ba/Ca analyses is ±3 % (1 SD, 131 degrees of freedom) based on 116 analyzed intervals.

4. RESULTS

4.1 *G. ruber* $\delta^{18}O$

The *G. ruber* $\delta^{18}O$ record shows an average Holocene value of –1.67 ‰. The record reaches a maximum value of –1.23 ‰ at 7.7 kyr and a minimum value of –2.07 ‰ at 8.0 kyr, with an overall variability of 0.84 ‰ (Figure 5). Through the high-resolution section of the record, there are significant enrichments in $\delta^{18}O$ at ~8.5, 7.7, and 6.6 kyr and depletions at ~8.0, 7.4, 6.8, 6.5, and 6.4 kyr. The lower resolution part of the record shows an enrichment at ~4.3 kyr that is followed within 100 yrs by an abrupt depletion in $\delta^{18}O$.

Lund and Curry [2006] measured $\delta^{18}O$ in *G. ruber* from the late Holocene in a core located about ten miles from JPC 51 in the same high sedimentation rate zone. Figure 6 shows a comparison between their *G. ruber* $\delta^{18}O$ record for the last 5.1 kyr and our record in JPC 51 (this study). The lower resolution section of our record shows a good match with their *G. ruber* $\delta^{18}O$ record from 5.1 kyr to the present. Age model error is most likely the limiting factor when comparing the two records, but the most striking feature of the two records is the agreement in the trend toward heavier values from ~3.2 to 2.2 kyr. Comparison of the early and late Holocene $\delta^{18}O$ records shows the presence of persistent millennial-scale climate cycles through the entire time interval. In addition, the overall minima *G. ruber* $\delta^{18}O$ values at ~3.0 kyr (for *Lund and Curry* [2006]) and from 6.4 – 6.8 and 7.6 – 7.9 kyr (for this study) as well as the maxima *G. ruber* $\delta^{18}O$ values at ~2 kyr (for *Lund and Curry* [2006]) and ~7.6 kyr (for this study) are in good agreement, suggesting persistent climate cycles throughout the Holocene (Figure 6).

4.2 Mg/Ca-SST

The Mg/Ca-SST record indicates a core top temperature of 27.3°C, in good agreement with the modern annual average SST of ~27.5°C in the Florida Straits [*Locarini et al.,* 2006] (Figure 2a). The early Holocene is marked by a warm interval from 8.1 to 7.9 kyr when temperatures reached 29.2°C. Following this warm interval, the record has a gradual cooling trend lasting ~1 kyr with the coolest temperatures of 27.2°C reached at 7.0 to 6.9 kyr. The high-resolution record then shows another warming trend with peak temperatures of just less than 29.0°C reached by 6.5 kyr. The lower-resolution part of the record also indicates similar temperature fluctuations in the Florida Straits over the last 6 kyr ranging from intervals as warm as ~29°C and as cool as 27°C.

4.3 $\delta^{18}O_{SW}$

Combining the Mg/Ca-SST estimates with the measured *G. ruber* $\delta^{18}O$ values, we calculated $\delta^{18}O_{SW}$ change in the Florida Straits over the last 9.1 kyr (Figure 7a). The average $\delta^{18}O_{SW}$ value is 1.03‰. The $\delta^{18}O_{SW}$ record shows a maximum value of 1.51‰ at 6.7 kyr and a minimum of 0.51‰ at 2.9 kyr. Therefore, the maximum amplitude of $\delta^{18}O_{SW}$ change is ~1.0‰ across the Holocene.

By subtracting average global $\delta^{18}O_{SW}$ change due to Holocene sea level rise (Figure 7b), we calculate the "ice volume free" $\delta^{18}O_{SW}$ record, hereafter referred to as $\delta^{18}O_{IVF\text{-}SW}$ (Figure 7c). The core top $\delta^{18}O_{IVF\text{-}SW}$ value is ~1 ‰, in good agreement with the modern average $\delta^{18}O_{SW}$ value in the Florida Straits of 0.95 ‰ [*Lund and Curry,* 2006]. During the early-mid Holocene, the record shows three clearly defined cycles

with $\delta^{18}O_{IVF\text{-}SW}$ values ranging from lows of 0.6‰ to highs of 1.4‰, resulting in a maximum amplitude of about 0.8‰ across each of these early Holocene events. The three periods of elevated early Holocene $\delta^{18}O_{IVF\text{-}SW}$ values are from 8.3 to 8.0 kyr, 7.6 to 7.4 kyr and from 6.6 to 6.3 kyr. In the lower resolution portion of the record, there are two prominent enrichments at 4.2 and 1.8 kyr.

4.4 Ba/Ca

Although most waters flowing through the Florida Straits today originate in the Caribbean, large riverine discharges from the Mississippi River may have impacted $\delta^{18}O_{SW}$ values at JPC 51 during the Holocene, occasionally complicating the $\delta^{18}O_{SW}$:SSS relationship at times in the past. This potential riverine impact was seen across the deglacial in the northern Gulf of Mexico by *Flower et al.* [2004] in a fossil *G. ruber* record of $\delta^{18}O_{SW}$ change. Compared to local precipitation ($\delta^{18}O$ = -7‰ [*Ortner et al.,* 1995]), meltwater discharges that originated from the Laurentide ice sheet had a much more negative $\delta^{18}O$ value during the deglacial (-25‰ to -35‰ [*Fairbanks*, 1989]). In their $\delta^{18}O_{SW}$ record from the Orca Basin, *Flower et al.* [2004] found evidence for a period of increased meltwater discharge into the Gulf of Mexico from about 16.5 to 13.0 kyr. They therefore argued that riverine discharge impacted on the local $\delta^{18}O_{SW}$:SSS relationship at their study site in the Orca Basin at this time, making it difficult to estimate SSS change from calculated $\delta^{18}O_{SW}$ values. Although the Florida Straits are located much further from the major sources of riverine input into the Gulf of Mexico and meltwater discharge during the Holocene was much smaller than during the

deglacial, we cannot rule out the possibility that river water with isotopically depleted $\delta^{18}O_{SW}$ values could have impacted our record from JPC 51.

The desorption of Ba^{2+} from suspended river sediments results in riverine Ba^{2+} concentrations higher in relation to seawater concentrations. Upon mixing in river estuaries, the dissolved Ba^{2+} concentrations conservatively mix with sea water, and results in an inverse linear relationship between salinity and Ba^{2+} [*Hanor and Chan*, 1977; *Edmond et al.,* 1978; *Coffey et al.,* 1997]. From laboratory experiments, live planktonic foraminifera linearly incorporate Ba^{2+} into their shells, primarily dependent upon the ambient seawater Ba^{2+} concentration [*Lea and Spero*, 1994; *Honisch et al.,* 2011]. Therefore, Ba/Ca ratios in foraminifera that calcify in a region of high dissolved [Ba^{2+}] input (such as the Mississippi River) can be used as a proxy for past SSS changes based on the regional $Ba_{seawater}$:SSS relationship. Even though modern average discharge rates from the Mississippi River are unlikely to directly impact SSS in the Florida Straits today, it is possible that higher discharge rates during major flooding or meltwater events during the Holocene may have had an impact on the region [*Walker et al.,* 2005].

In order to identify the timing of increased riverine influence on surface salinity in the Florida Straits, we measured Ba/Ca ratios in the same *G. ruber* shell material from JPC 51 (Figure 7d). The input of isotopically depleted river water into the Gulf of Mexico could potentially cause a large change in $\delta^{18}O_{SW}$ with only a small change in SSS, so we use the Ba/Ca record in conjunction with the $\delta^{18}O_{IVF\text{-}SW}$ record to identify periods when the $\delta^{18}O_{IVF\text{-}SW}$ values may have been significantly influence by riverine

input. Therefore, we can identify periods in the JPC 51 $\delta^{18}O_{IVF\text{-}SW}$ record when the changes are more like due to elevated riverine input rather than regional variations in E/P ratios (atmospheric circulation driven).

Using end member [Ba^{2+}] in the modern Gulf of Mexico of 11.2 μg/L [*Hanor and Chan*, 1977] and in the northern Caribbean is 8.5 μg/L [*Turekian and Johnson,* 1966], we estimate a modern [Ba^{2+}] of 9.0 to 10.0 μg/L for the Florida Straits. With this estimation, along with the empirical relationship in *Lea and Spero* [1994] the calculated shell Ba/Ca ratio in equilibrium with this modern water mass would be ~0.95 μmol/mol, in excellent agreement with the average Ba/Ca ratio of ~0.95 μmol/mol in the entire JPC 51 Holocene record (Figure 7d). Using this value as a baseline to identify periods of elevated [Ba^{2+}] input into the Gulf of Mexico across the Holocene, the high-resolution record shows four peaks that stand out above background levels centered at ~8.2, 7.6, 7.0 and 6.6 kyr when Ba/Ca ratios exceed 1.1 μmol/mol. These individual peaks in the Ba/Ca record are single-point jumps, but the data have been replicated at least two to three times and are therefore reproducible and stand above the pooled standard deviation value of ±3 %, indicating they are statistically significant. Although it is possible that $\delta^{18}O_{SW}$ values were influenced by isotopically depleted riverine water during these four brief intervals, it is interesting to note that only the Ba/Ca peak at 7.0 kyr is associated with light $\delta^{18}O_{SW}$ values (Figure 7c and d). This suggests that riverine input did not have a significant impact on our $\delta^{18}O_{SW}$ record from JPC 51. Instead, the major driver of Holocene $\delta^{18}O_{SW}$ change in the Florida Straits must be due to regional changes in E/P associated with hydrologic cycle variability.

4.5 Conversion of $\delta^{18}O_{IVF\text{-}SW}$ to SSS

Using the modern tropical Atlantic $\delta^{18}O_{SW}$: SSS relationship [*Schmidt et al.*, 1999],

$$\delta^{18}O_{SW}\ (‰) = 0.26*S(psu) - 8.44 \qquad \text{(Eq. 3)}$$

we calculate a core top salinity of 36.0. This agrees well with the average annual salinity value of ~36.0 for the Florida Straits reported by *Antonov et al*. [2006](Figure 2b). Based on this modern regression, a change of 0.26 ‰ in $\delta^{18}O_{SW}$ is equivalent to a change in SSS of 1. Based on the modern relationship, the calculated $\delta^{18}O_{IVF\text{-}SW}$ values from JPC 51 suggest Holocene SSS changes ranging from 34.4 to 38.2 with an average of 36.2. Given that this range in SSS seems too large for realistic Holocene SSS variability in the Florida Straits, it is likely that the slope of the $\delta^{18}O_{SW}$: SSS relationship must have changed over the Holocene. Based on the results of a coupled GCM modeling study, *Oppo et al.* [2007] found significant changes in the tropical hydrologic cycle associated with orbital changes in solar insolation during the mid Holocene. Their results suggest a decrease in the water vapor transport across the Central American Isthmus during the mid Holocene resulting from a northward shift in the position of the ITCZ and a decrease in the Pacific easterlies at that time. Because water vapor transported from the Atlantic to the Pacific via the trade winds is isotopically depleted, a decrease in the net transport results in a decrease in $\delta^{18}O_{PRECIPITATION}$ values in the western tropical Atlantic during the mid Holocene. More negative $\delta^{18}O_{PRECIPITATION}$ values in the circum-Caribbean region would result in a steeper $\delta^{18}O_{SW}$:SSS

relationship, thus reducing the magnitude of SSS change estimated from our $\delta^{18}O_{IVF\text{-}SW}$ record for the early to mid Holocene.

4.6 Evaluating the Proposed Salinity Effect on Shell Mg/Ca ratios

A recent study by *Arbuszewski et al.* [2010] suggests that past changes in SSS, in addition to SST change, can affect foraminiferal shell Mg/Ca ratios. This study proposes the use of multivariate equations to calculate past SST and SSS change from foraminiferal shell material. They derived the following equations to solve for SST and SSS:

$$SST = 16.06 + 4.62*\ln(Mg/Ca) - 3.42*(\delta^{18}O_{Shell}) - 0.1\ (\Delta CO_3^{2-}) \quad \text{(Eq. 4)}$$

$$SSS = 34.28 + 1.97*\ln(Mg/Ca) + 0.59*(\delta^{18}O_{Shell}) \quad \text{(Eq. 5)}$$

Because our core represents such a shallow depth, the effect of bottom water (ΔCO_3^{2-}) change is negligible. By using this calculation with our data, the results yield a range of SST values from 27.5°C to 30.6°C, which on average results in a SST record that is 0.8°C warmer than the record generated using Equation 2 (Figure 8). In addition, use of the multivariate equation calculates a core top temperature of 28.4°C, almost 1°C warmer than the modern annual average SST in the Florida Straits. This would imply the *G. ruber* Mg/Ca-SST record is heavily biased toward the warmest months of the year and can only be used as a proxy for summer conditions in the Florida Straits. The multivariate SST equation also results in unrealistically warm SST estimates for the last 3 kyr, suggesting that SSTs were as warm as 30 °C from 3.5 – 2.8 kyr, and then cooled by 2°C over the last 2.8 kyr. This amount of cooling over the last 2.8 kyr seems unrealistically large, given that the total amount of cooling during the LGM at this site is

estimated to have only been only ~3 ºC at the LGM based on the results of the MARGO project [*Waelbroeck et al.*, 2009]. Therefore, we have more confidence in the SST record generated using the traditional approach based on the *Anand et al.* [2003] relationship (Equation 2).

In order to determine how the new multivariate equation would affect the timing of our estimated SSS change, we show a comparison of SSS calculated using multivariate Equation 4 and the $\delta^{18}O_{IVF\text{-}SW}$ record calculated using the traditional method with Equations 1 and 2 (Figure 9). The core top SSS calculated for JPC 51using the multivariate equations is 36.3, 0.3 higher than the modern average SSS and is very close to the modern yearly maximum SSS in the Florida Straits. In fact, the SSS record calculated using the multivariate equation suggests higher than modern SSS values in the Florida Straits over the entire Holocene, ranging from 36.0 to 36.8. Although the multivariate and the traditional method of calculating $\delta^{18}O_{IVF\text{-}SW}$ using Equations 1 and 2 imply different magnitudes of SSS variation across the Holocene, the implied SSS changes in the high-resolution part of our record from the early to mid Holocene are nearly synchronous (Figure 9). Both records indicate three periods of elevated SSS in the Florida Straits from 8.3 to 8.0 kyr, 7.6 to 7.4 kyr and from 6.6 to 6.3 kyr. Therefore, even if the salinity effect on foraminiferal Mg/Ca values is correct, the use of these equations does not change the timing of the implied SSS change in our record.

5. DISCUSSION

5.1 Holocene SST Record

The reconstructed Mg/Ca-SST record from the Florida Straits indicates only a ~0.8°C cooling trend through the Holocene. Local spring-summer insolation has gradually decreased during the Holocene (~25 W/m^2) due to precessional changes in the seasonal distribution of insolation (Figure 10). Therefore, it is possible that orbital-scale changes in the local spring and summer insolation caused by precession could be the driver of this Holocene SST cooling trend. However, the small magnitude of Holocene cooling observed in the JPC 51 record suggests the change in seasonality across the Holocene did not have a dramatic affect on the *G. ruber* SST record. This may be evidence that *G. ruber* flux in the Florida Strait is not heavily biased toward summer months, but instead remains relatively constant throughout the annual cycle.

LoDico et al. [2006] published a high-resolution (~30 yr sample spacing) SST reconstruction from the northern Gulf of Mexico's Orca Basin spanning from 10.5 to 7.0 kyr based on Mg/Ca ratios in *G. ruber* (white variety). However, *LoDico et al.* [2006] did not use the reductive cleaning step in their methods. Because the reductive cleaning step in the Mg/Ca cleaning protocol has been shown to lower shell Mg/Ca ratios by 10% [*Pena et al.,* 2005], we decreased their reported Mg/Ca values by 10% to make them more comparable to the results in this study. We also updated the age model for the *LoDico et al.* [2006] record by recalibrating their radiocarbon dates using CALIB 6.0 (Figure 11).

The *LoDico et al.* [2006] SST record indicates an abrupt warming at ~9.4 kyr, followed by millennial-scale oscillations of ~1.0°C (Figure 11). In contrast, the Florida Straits SST record indicates warmer conditions during the early Holocene from 9.2 to 8.0 kyr where the two records overlap. Similar SSTs are recorded at both sites from 7.8 to 7.3 kyr. While the Florida Straits record shows early Holocene centennial-scale SST cycles that are similar in magnitude to those reconstructed for the Orca Basin, the timing of these oscillations is not the same.

The greatest difference between the Florida Straits and Orca Basin SST records occurs between ~8.8 to 8.6 kyr and from ~8.2 to 7.8 kyr. It is possible that the different temperature evolution between the two sites is because that the northern Gulf of Mexico is more directly influenced by North American climate whereas hydrographic conditions in the Florida Straits are more influenced by the waters associated from the western tropical Atlantic [*Schmitz and Richardson*, 1991]. This may explain why the Orca Basin records a cooling during the 8.2 kyr event, but the Florida Straits does not. The 8.2 kyr event is thought to be the largest climate anomaly of the entire Holocene [*Alley and Agustsdottir*, 2005]. It is possible that this high latitude cool period resulted in cooler surface temperatures over much of North America. Therefore the significant cooling recorded in the Orca Basin around 8.2 kyr most likely reflects the influence of cooler temperatures over the interior North American continent, while the warmer SSTs in the Florida Straits suggest the tropics were less affected by the high latitude cooling and possibly are less sensitive to SST in general.

To determine the presence, frequency and duration of sub-orbital cycles in our Holocene SST record, we analyzed the record using wavelet analysis [*Grinsted et al.,* 2004]. We performed two separate analyses on the SST record, one spanning the entire Holocene section of our record and the other spanning just the high-resolution part of the record from the early Holocene (9.1 to 6.2 kyr). The early Holocene analysis (Figure 12a) was interpolated at 30 yr intervals, coincident with the high-resolution sampling time steps, while the entire Holocene analysis (Figure 13b) was interpolated at 150-year intervals, consistent with the maximum spacing between sample intervals. In the early Holocene analysis (Figure 12a), strong spectral power above the 95% confidence level is indicated at 70, 125 and 800-year periods. However, spectral power at the 70 year interval is limited to 8.8 kyr and from 7.6 – 7.5 kyr and spectral power at the 125 year period is limited to two brief intervals from 8.4 – 8.3 and from 7.3 – 7.1 kyr. Spectral power at the 70 year period suggests a possible link to the internally forced Atlantic multidecadal oscillation (AMO) (30-80 year period) [*Dima and Lohmann*, 2007] which some modeling studies suggest is the result of high-frequency AMOC variability during the Holocene [*Delworth and Mann,* 2000; *Enfield et al.*, 2001; *Heslop and Paul,* 2011]. The most persistent period through the early Holocene SST record is at 800 years, although the length of our record limits our ability to confirm this cycle beyond the period from 8.2-7.5 kyr. In the lower-resolution Holocene analysis (Figure 12b) spectral power above the 95% confidence level occurs at the 600-year period briefly around 7.0 kyr. The most persistent period through the complete low-resolution Holocene SST record is at the 2,000-year period.

5.2 Holocene $\delta^{18}O_{IVF\text{-}SW}$ and Salinity Variability

First, we compare the JPC 51 early Holocene record of $\delta^{18}O_{IVF\text{-}SW}$ with the previously published late Holocene $\delta^{18}O_{IVF\text{-}SW}$ record from Florida Straits core 79 GGC [*Lund and Curry* 2006]. Core 79 GGC is located very close to JPC 51 and the $\delta^{18}O_{IVF\text{-}SW}$ record was calculated using the same methodologies and calibration equations used in this study. Comparison of the two records shows that both periods were characterized by similar magnitude $\delta^{18}O_{IVF\text{-}SW}$ oscillations with almost the same average value (the two red curves in Figure 13b). In their study, *Lund and Curry* [2006] found fresher conditions in the Florida Straits during the Medieval Warm Period (MWP) and saltier surface conditions during the Little Ice Age (LIA). They argued that the development of elevated $\delta^{18}O_{SW}$ values (and higher SSS) in the Florida Straits during the LIA resulted from increased E/P ratios in the northern tropical Atlantic associated with a southward shift in the Hadley cell circulation and the ITCZ, as recorded in the percent titanium record from the Cariaco Basin (Figure 13b, c). Ostracod $\delta^{18}O$ records from Haitian lake cores indicate wetter conditions in the northern Caribbean during the early Holocene [*Hodell et al.,* 1991] and faunal census studies from Gulf of Mexico sediment cores suggest the loop current penetrated farther north [*Poore et al.,* 2003]. *Poore et al.* [2003] argued that greater loop current penetration into the Gulf of Mexico during the early Holocene is evidence for a more northerly position of the ITCZ over the Caribbean. In comparison, titanium records from the Cariaco Basin (northern Venezuela) suggests that rainfall amounts over northern South America were at a maximum during the early Holocene, most likely caused by a more intense ITCZ located

farthest to the north [*Haug et al.,* 2001] (Figure 13c). Although the JPC 51 record indicates large $\delta^{18}O_{IVF\text{-}SW}$ oscillations during the early Holocene that are similar in magnitude with those recorded in the late Holocene [*Lund and Curry,* 2006], the $\delta^{18}O_{IVF\text{-}SW}$ oscillations from 9.2 to 6.2 kyr do not correlate with changes in the Cariaco Basin percent titanium record (Figure 13b, c). Unlike other study locations nearby in the Gulf of Mexico (*Poore et al.*, 2003), this suggests the early Holocene $\delta^{18}O_{IVF\text{-}SW}$ cycles in the Florida Straits cannot be simply explained by meridional shifts in the ITCZ.

Second, we compare our early Holocene $\delta^{18}O_{IVF\text{-}SW}$ record with a similar resolution $\delta^{18}O_{IVF\text{-}SW}$ reconstruction from the northern Gulf of Mexico's Orca Basin (gray curve on Figure 13b) [*LoDico et al.,* 2006]. In order to directly compare the JPC 51 $\delta^{18}O_{IVF\text{-}SW}$ reconstruction with the Orca Basin record, we recalculated their data using Equations 1 and 2 and then corrected the resulting $\delta^{18}O_{sw}$ values for continental ice volume variability using the same global seawater $\delta^{18}O$ record shown on Figure 7b. Overall, there is a remarkable match between the calculated $\delta^{18}O_{IVF\text{-}SW}$ values from both locations, especially between 9.2 to 8.6 kyr and again from 7.8 to 7.1 kyr (Figure 13b). However, the Orca Basin $\delta^{18}O_{IVF\text{-}SW}$ record indicates two significant freshening events between 8.4 and 8.0 kyr that are not recorded in the JPC 51 record. Just as the SST comparison between the Orca Basin and the Florida Straits indicates the development of a steep temperature gradient across the Gulf of Mexico associated with the 8.2 kyr event (Figure 11), the $\delta^{18}O_{IVF\text{-}SW}$ comparison suggests large differences in SSS between the two sites as well. The cool, fresh conditions in the northern Gulf of Mexico associated with the 8.2 kyr event apparently did not extend into the Florida Straits.

If the 8.2 kyr cool period resulted in elevated Mississippi River discharge into the Gulf of Mexico, as suggested by the *LoDico et al.* [2006] $\delta^{18}O_{IVF\text{-}SW}$ record, then it is possible that river water with depleted oxygen isotope values could have influenced $\delta^{18}O_{SW}$ values in the Florida Straits as well. The JPC 51 Ba/Ca record shows three statistically significant one-point peaks in Ba/Ca that stand out above estimated modern value in the Florida Straits of 0.95 μmol/mol (Figure 13a). These Ba/Ca peaks occur at 8.2, 7.6 and 7.0 kyr. It is interesting to note that the first two peaks at 8.2 and 7.6 kyr do not correspond with light $\delta^{18}O_{SW\text{-}IVF}$ values in the Florida Straits, but instead correspond to light $\delta^{18}O_{IVF\text{-}SW}$ values in the Orca Basin record. This lends support to the interpretation that the negative $\delta^{18}O_{IVF\text{-}SW}$ excursions in the Orca Basin record do reflect elevated riverine input into the northern Gulf of Mexico. However, the relatively small and brief increases in Ba/Ca ratios in JPC 51 suggests the impact of these northern Gulf of Mexico riverine injections on SSS in the Florida Straits was minor. Therefore, while riverine discharge associated with the 8.2 kyr event most likely affected surface salinities in the Orca Basin, the enriched $\delta^{18}O_{IVF\text{-}SW}$ values in the Florida straits at this time suggest an increase in tropical Atlantic E/P ratios, most likely associated with more arid conditions over the western tropical Atlantic.

Several studies suggest the major driver of early Holocene climate change on centennial to millennial time scales is solar output variability [*Bond et al.,* 1997; *Bond et al.,* 2001; *Lund and Curry,* 2004; *Roth and Reijmer,* 2005; *Lund and Curry,* 2006; *LoDico et al.,* 2006; *Saenger et al.,* 2009, *Marchitto et al.,* 2010]. The impact of solar variability on Holocene climate was made clear when *Bond et al.* [2001] found increases

in ice rafted debris (IRD) in North Atlantic sediments about every 1500 years, suggesting periods of cooler temperatures in the high-latitude North Atlantic. *Bond et al.* [2001] showed that intervals associated with increased IRD correspond to periods of elevated ^{14}C production in the atmosphere. More ^{14}C is produced in the atmosphere during periods of reduced solar winds, so periods of increased IRD occur during intervals of reduced solar output.

Furthermore, several ocean-atmosphere modeling studies point to the tropical Pacific as playing a major role in driving sub orbital-scale climate variability [*Bush and Philander,* 1998; *Cane*, 1998; *Cane and Clement*, 1999; *Clement et al.,* 1999; *Kukla et al.,* 2002]. These studies suggest that ENSO is controlled by changes in seasonal cycle forcing at the equator, correlating periods of reduced solar irradiance (decreased seasonality) with stronger El Niño forcing. According to the Zebiak-Cane model of ENSO dynamics, relatively small changes in total irradiance can cause the background state of the tropical Pacific to oscillate between El Niño/La Nina states [*Mann et al.,* 2005].

A recent study by *Marchitto et al.* [2010] showed that changes in solar output during the early Holocene had a large impact on El Niño/Southern Oscillation (ENSO) variability in the eastern equatorial Pacific (EEP). *Marchitto et al.* [2010] reconstructed Holocene SST anomalies off the coast of Baja California Sur, Mexico in the Soledad Basin using Mg/Ca ratios in the planktonic foraminifera *Globigerinoides bulloides*. *Marchitto et al.* [2010] first smoothed their Mg/Ca-SST anomaly record using a 250-year running mean in order to remove high-frequency climate variability that cannot be

reliably correlated with other proxy records (Figure 14b). They then smoothed the Holocene records of ^{14}C [*Reimer et al.*, 2004] and ^{10}Be production [*Finkel and Nishiizumi*, 1997; and *Vonmoos et al.*, 2006] using the same 250-year running mean and then removed the long-term drift in the nuclide records resulting from slow variations in the Earth's geomagnetic field [*Wagner et al.,* 2000] by performing a highpass filter at 1/1800-year (Figure 14e and f). This same highpass filter was used by *Bond et al.,* [2001] to generate their stacked IRD record shown on Figure 14d. As a result, *Marchitto et al.* [2010] identified 5 warm intervals between 11 to 7 kyr (more El Niño-like conditions) separated by roughly 1 kyr that corresponded to periods of increased ^{14}C and ^{10}Be production (times of reduced solar activity). *Marchitto et al.* [2010] argued that centennial-scale changes in solar output resulted in stronger El Niño forcing in the tropical Pacific during times of reduced solar output. Comparison of their new SST record from 6.5 - 14 kyr with *Bond et al.* [2001]'s IRD record (Figure 14d) also showed a strong correlation between cool periods in the North Atlantic and more El Niño-like conditions in the EEP (Figure 14b).

In the Florida Straits, we find evidence for increased SSS (more positive $\delta^{18}O_{IVF-SW}$ values) associated with North Atlantic cooling and the development of El Niño-like conditions in the EEP. Comparison of the JPC 51 $\delta^{18}O_{IVF-SW}$ record (smoothed with a 250-year running mean to make it comparable with the data from *Marchitto et al.* [2010]) with proxies for solar variability shows a correlation between increased ^{14}C and ^{10}Be production and positive $\delta^{18}O_{IVF-SW}$ values in the Florida Straits (Figure 14a, e and f) (^{14}C: $r = 0.38$, $p = 0.0041$; ^{10}Be: $r = 0.41$, $p = 0.0019$) (Table 2). *Bond et al,* [2001]

showed that IRD content in the North Atlantic increased during periods of reduced solar output and we find that periods of increased IRD also correlate to elevated $\delta^{18}O_{IVF\text{-}SW}$ values in the Florida Straits ($r = 0.44$, $p < 0.001$, with 100-year lag). Therefore, cool periods in the high-latitude North Atlantic are associated with drier conditions in the tropical North Atlantic during the early Holocene.

Although the overlap between the Soledad Basin Mg/Ca-SST anomaly record and the JPC 51 $\delta^{18}O_{IVF\text{-}SW}$ record only spans ~2.6 kyr, the two records have the best correlation ($r = 0.74$, $p << 0.001$) (Table 2) (Figure 14a and b), suggesting a tight coupling between ENSO changes in the EEP and E/P ratios in the western tropical Atlantic. Finally, speleothem oxygen isotope records from Dongge Cave (southern China, *Wang et al.,* 2005) show the Asian monsoon system weakens during periods of reduced solar output. Comparison of the Dongge Cave oxygen isotope record with the JPC 51 $\delta^{18}O_{IVF\text{-}SW}$ record shows that a weaker Asian monsoon is also correlated with drier conditions in the Florida Straits ($r = 0.58$, $p < 0.001$) (Table 2) (Figure 14a and c). Therefore, the correlation between the Florida Straits $\delta^{18}O_{IVF\text{-}SW}$ record from the tropical Atlantic with the Soledad Basin Mg/Ca-SST anomaly record from the EEP and the Dongge Cave oxygen isotope record from southern China suggest a dramatic reorganization of atmospheric circulation patterns around the globe driven by changes in Holocene solar output.

It is not surprising that more permanent El Niño-like conditions in the EEP are associated with a more arid circum-Caribbean climate. ENSO variability directly impacts climate in the north Atlantic, resulting in reduced rainfall, warmer SSTs, and

weaker trade winds in the western tropical north Atlantic during an El Niño [*Poveda and Mesa*, 1997; *Giannini et al.,* 2001; *Alexander et al.,* 2002; *Alexander and Scott,* 2002]. Based on coupled ocean-atmosphere general climate model results [*Latif*, 2000; *Schmittner and Clement*, 2002] and reanalysis of two historical data sets [*Schmittner et al.,* 2000], El Niño conditions result in enhanced water vapor transport from the tropical Atlantic to the Pacific. It has even been hypothesized that if these freshwater perturbations associated with an El Niño persisted for longer than a few decades, they could have significantly impacted AMOC by increasing Atlantic SSS [*Schmittner et al.,* 2000; *Schmittner and Clement*, 2002].

Furthermore, *Saenger et al.* [2009] used a coupled global circulation model to isolate the impact of high latitude cooling on the tropical Atlantic hydrologic cycle. Their results show that a 2°C cooling in the North Atlantic results in increased wind stress and precipitation anomalies in the tropical North Atlantic. The high latitude cooling increases the strength of the northeast trade winds, resulting in increased evaporation rates in the tropical Atlantic. Therefore, the elevated $\delta^{18}O_{IVF\text{-}SW}$ values in JPC 51 associated with increased North Atlantic IRD (and a cooler North Atlantic) are consistent with this high-to-low latitude climate teleconnection, reflecting increased E/P ratios in the Florida Straits during periods of high-latitude cooling.

Although we cannot determine whether forcing from the tropical Pacific (ENSO) or the high-latitude North Atlantic had the strongest impact on the tropical Atlantic hydrologic cycle, the strong cooling in the North Atlantic associated with the 8.2 kyr event seems to have locked the tropical hydrologic cycle into a 'cold phase.' During the

8.2 kyr event, the final drainage of large pro-glacial lakes into the North Atlantic is thought to have resulted in a meltwater-induced reduction in Atlantic meridional overturning circulation that caused widespread cooling in the circum-Atlantic region [*Barber et al.,* 1999; *Fisher et al.,* 2002; *Clark et al.,* 2004; *Alley and Agustsdottir,* 2005; *Ellison et al.,* 2006]. Although the JPC 51 $\delta^{18}O_{IVF\text{-}SW}$ record covaries with changes in solar output across two complete cycles (~7.4 to 6.2 kyr and 8.0 to 7.4 kyr), the correlation decreases during the interval around the 8.2 kyr event (grey bar on Figure 14). Because the 8.2 kyr event was forced by an internal driver rather than by changes in solar variability, it is not surprising that JPC 51 $\delta^{18}O_{IVF\text{-}SW}$ record does not match the solar output proxy. Instead, the JPC 51 $\delta^{18}O_{IVF\text{-}SW}$ record shows a much better correlation with the Soledad Basin SST-anomalies and the Dongge Cave record because these records reflect a teleconnected response to the high latitude cooling associated with the 8.2 kyr event and a disconnect to variability in solar output. The 8.2 kyr event occurs at a time of increasing solar activity, but SSS remained elevated in the Florida Straits, SST's in the EEP remained warm and the Asian monsoon remained weak. This suggests the cool conditions in the North Atlantic caused by freshwater forcing prevented the tropics from responding to the increase in solar activity at this time.

To determine the frequency of sub-orbital cycles in our Holocene $\delta^{18}O_{IVF\text{-}SW}$ record, we calculated a wavelet analysis [*Grinsted et al.,* 2004] of our data. Again, we conducted two wavelet analyses, one of the high-resolution early Holocene data from 9.1 to 6.2 kyr using a 30 year interpolation (Figure 15a), and the other over the entire Holocene using a 150 year interpolation (Figure 15b). The high-resolution early

Holocene analysis shows strong spectral power at ~800 and 70-year periods, both above the 95% confidence level (Figure 15a). This analysis also indicates spectral power at the 200-year period before 7.0 kyr. Strong spectral power is only found at the 2000-year period in the lower resolution record from 6.0 - 4.5 kyr (above the 95% confidence level) (Figure 15b).

We also performed a spectral analysis of the high-resolution section of the JPC 51 $\delta^{18}O_{IVF-SW}$ record (9.1 to 6.2 kyr) (Figure 16). This analysis reveals peaks at periods of 600, 200 and 70 years, all above the 95% confidence level. Spectral power at the 200 year period is common in proxies forced by solar variability, reflecting the ~200 year Suess or Devries solar cycle [*Stuiver and Braziunas*, 1991]. Previous studies showed prominent 200-year cycles in records from Central American lakes [*Curtis et al.,* 1996; *Hodell et al.,* 2001] and in Cariaco Basin foraminiferal faunal variability [*Peterson et al.,* 1991]. Although near the limit of what our record can resolve, the peak at the 70 year period reinforces our wavelet analysis of the SST data described at the conclusion of Section 5.1. *Knight et al.* [2006] showed that the warm AMO phase is associated with a northward displacement of the ITCZ over the tropical Atlantic, suggesting a possible influence of the AMO on the tropical Hydrologic cycle.

Finally, we computed cross wavelet transforms [*Grinsted et al.,* 2004] to identify common spectral power and its phase relationship between the unsmoothed, high-resolution JPC 51 $\delta^{18}O_{IVF-SW}$ record and the ^{14}C and ^{10}Be proxies (Figure 17a and b). Therefore, these transforms only span the early Holocene from 9.1 to 6.2 kyr. The data were first interpolated to constant 30 year spacing for all records (based on the average

spacing of the JPC 51 $\delta^{18}O_{IVF\text{-}SW}$ record for this time interval). The strongest common power in both cross wavelet transforms is at periods of about 0.8 to 1 kyr. At these periods, there is a 0º phase angle and the common power is above the 95% confidence interval. The JPC 51 $\delta^{18}O_{IVF\text{-}SW}$ record and the ^{14}C production record share common power above the 95 % confidence interval at periods of 0.2 and 0.07 kyr (Figure 17a). Significant common power extends forward to ~8.1 kyr at the 0.2 kyr period with a phase angle of nearly 180º. After ~8.0 kyr, significant common power is shared at the 0.07 kyr period with a phase angle of 90º. The cross wavelet transform with the ^{10}Be record also shows significant common power at the 70 year period extending forward of ~8.0 kyr as well as shared common power at the 200-year period before ~8.1 kyr (although spectral power at this period is below the 95% confidence level). As noted above, the 200-year period is a dominant solar cycle, suggesting that solar forcing is a significant driver of early Holocene tropical hydrologic variability on centennial time scales.

6. CONCLUSIONS

Our new Mg/Ca-SST record from the Florida Straits indicates only a small (~0.8°C) cooling trend through the Holocene. While the Florida Straits record shows early Holocene centennial-scale SST cycles that are similar in magnitude to those previously reconstructed for the Orca Basin over the same time interval, the timing of these oscillations is not the same. The greatest difference between the Florida Straits and Orca Basin SST records occurs from ~8.8 to 8.6 kyr and from ~8.2 to 7.8 kyr. We conclude that the different temperature evolution between the two sites is due to the fact that the northern Gulf of Mexico is more directly influenced by North American climate whereas hydrographic conditions in the Florida Straits are more influenced by the waters associated from the western tropical Atlantic traveling through the Caribbean and Yucatan Channel to the core site.

After correcting our calculated $\delta^{18}O_{SW}$ record for global changes in $\delta^{18}O_{SW}$ due to continental ice volume variability, the ice volume free $\delta^{18}O_{SW}$ record from the Florida Straits shows centennial-scale oscillations on the order of 0.4‰. Comparison of our early Holocene $\delta^{18}O_{IVF\text{-}SW}$ record with the late Holocene $\delta^{18}O_{IVF\text{-}SW}$ reconstruction from the same location in the Florida Straits shows that both periods were characterized by similar magnitude $\delta^{18}O_{IVF\text{-}SW}$ variability. Although the late Holocene $\delta^{18}O_{IVF\text{-}SW}$ oscillations correlate with meridional shifts in the position of the ITCZ, the $\delta^{18}O_{IVF\text{-}SW}$ oscillations during the early Holocene do not show a strong connection to ITCZ shifts.

Instead, we find evidence for increased SSS (more positive $\delta^{18}O_{IVF\text{-}SW}$ values) associated with North Atlantic cooling and the development of El Niño-like conditions

in the EEP that are driven by changes in solar irradiance. As solar output cycles reached a minimum during the early Holocene, proxy records from the EEP suggest the development of more permanent El Niño -like conditions and Chinese speleothem records indicate intervals of a weakened Asian Monsoon. At the same time, these events were also associated with elevated SSS in the Florida Straits, providing evidence for a dramatic reorganization of atmospheric circulation patterns around the globe driven by Holocene changes in solar output.

Finally, we show that the strong cooling in the North Atlantic associated with the 8.2 kyr event seems to have locked the tropical hydrologic cycle into a 'cold phase.' Because the 8.2 kyr event was forced by an internal driver rather than by changes in solar variability, the JPC 51 $\delta^{18}O_{IVF\text{-}SW}$ record reflects a teleconnected response to the high latitude cooling at 8.2 kyr. Although nuclide records suggest solar irradiance was increasing at the start of the 8.2 kyr event, SSS remained elevated in the Florida Straits for several hundred years after the meltwater-induced collapse of AMOC. This suggests a strong coupling between high-latitude North Atlantic climate and the tropical Atlantic hydrologic cycle.

REFERENCES

Alexander, M. and J. Scott, (2002), The influence of ENSO on air-sea interactions in the Atlantic, *Geophysical Research Letters, 29*, 1701, doi:10.1029/2001GL014347

Alexander, M. A., I. Blade, M. Newman, J. R. Lazante, N.-C. Lau, and J. D. Scott (2002), The atmospheric bridge: The influence of ENSO teleconnections on air-sea interaction over the global oceans. *Journal of Climate*, *15*, 2205-2231.

Alley, R. B., and A. M. Agustsdottir (2005), The 8k event: Cause and consequences of a major Holocene abrupt climate change, *Quaternary Science Reviews*, *24*(10-11), 1123-1149.

Anand, P. H. Elderfield, and M. H. Conte (2003), Calibration of Mg/Ca thermometry in planktonic foraminifera from a sediment trap time series, *Paleoceanography*, *18*, 1-15.

Antonov, J. I., R. A. Locarnini, T. P. Boyer, A. V. Mishonov, and H. E. Garcia (2006), *World Ocean Atlas 2005, Volume 2: Salinity*. S. Levitus, Ed. NOAA Atlas NESDIS 62, 182 pp, U.S. Government Printing Office, Washington, D.C.

Arbuszewski, J. A., P. deMonocal, A. Kaplan, and E. C. Farmer (2010), On the fidelity of shell-derived $\delta^{18}O$ seawater estimates, *Earth and Planetary Science Letters, 300,* 185-196.

Barber, D. C., A. Dyke, C. Hillaire-Marcel, A. E. Jennings, J. T. Andrews, M. W. Kerwin, G. Bilodeau, R. McNeely, J. Southon, M. D. Morehead, and J.-M. Gagnon (1999), Forcing of the cold event of 8,200 years ago by catastrophic drainage of Laurentide lakes, *Nature*, *400*(6742), 344-348.

Bard, E., B. Hamelin, R. G. Fairbanks, and A. Zindler (1990), Calibration of the C-14 timescale over the past 30,000 years using mass-spectrometric U-Th ages from the Barbados corals, *Nature*, *345*(6274), 405-410.

Bé, A. W. H., and D. S. Tolderlund (1971), Distribution and ecology of living planktonic foraminifera in surface waters of the Atlantic and Indian Oceans, in *Micropaleontology of Oceans*, edited by B. M. Funnell and W. R. Riedel, 105–149, Cambridge University Press, New York.

Bemis, B. E., H. J. Spero, J. Bijma, and D. W. Lea (1998), Reevaluation of the oxygen isotopic composition of planktonic foraminifera: Experimental results and revised paleotemperature equations, *Paleoceanography*, *13*(2), 150-160.

Bond, G., W. Showers, M. Cheseby, R. Lotti, P. Almasi, P. deMenocal, P. Priore, H. Cullen, I. Hajdas, and G. Bonani (1997), A pervasive millennial-scale cycle in North Atlantic Holocene and glacial climates, *Science 278*(14), 1257-1266.

Bond, G., B. Kromer, J. Beer, R. Muscheler, M. N. Evans, W. Showers, S. Hoffman, R. Lotti-Bond, I. Hajdas, and G. Bonani (2001), Persistent solar influence on north Atlantic climate during the Holocene, *Science*, *294*(5549), 2130-2136.

Boussetta, S., F. Bassinot, A. Sabbatini, N. Caillon, J. Nouet, N. Kallel, H. Rebaubier, G. Klinkhammer, and L. Labeyrie (2011), Diagenetic Mg-rich calcite in Mediterranean sediments: Quantification and impact on Mg/Ca thermometry, *Marine Geology* (280), 195-204.

Brown, S. J., and H. Elderfield, (1996), Variations in Mg/Ca and Sr/Ca ratios of planktonic foraminifera caused by post depositional dissolution: Evidence of shallow Mg-dependent dissolution, *Paleoceanography*, *11*, 543–551.

Brunner, C. A. (1982), Paleo-oceanography of surface waters in the Gulf of Mexico during the Late Quaternary, *Quaternary Research*, *17*(1), 105-119.

Bush, A. B. G. and S. G. H. Philander (1998), The role of ocean-atmosphere interactions in tropical cooling since the last glacial maximum, *Science, 279,* 1341-1344.

Cane, M. A. (1999), Climate change – a role for the tropical Pacific, *Science, 282*, 59-61.

Cane, M. A. and A.C. Clement (1999), A role for the Tropical Pacific coupled ocean-atmosphere system on Milankovich and millenial timescales, Part II: Global impacts, in *Mechanisms of Global Climate Change at Millenial Timescales*, edited by P. U. Clark, et al., 373-383, American Geophysical Union, Washington D. C.

Clement, A.C., and M. A. Cane (1999), A role for the Tropiical Pacific coupled ocean-atmosphere system on Milankovich and millenial timescales, Part I: A Modeling Study of Tropical Pacific Variability, in *Mechanisms of Global Climate Change at Millenial Timescales*, edited by P. U. Clark, et al., 363-371, American Geophysical Union, Washington D. C.

Clement, A. C., R. Seager, and M. A. Cane (1999), Orbital controls on the El Nino/Southern Oscillation and the tropical climate, *Paleoceanography, 14*, 441-456.

Clark, P. U., A. M. McCabe, A. C. Mix, and A. J. Weaver (2004), Rapid rise of sea level 19,000 years ago and its global implications, *Science*, *304*(5674), 1141-1144.

Coffey, M., F. Dehairs, O. Collette, G. Luther, T. Church, and T. Jickells (1997), The behaviour of dissolved barium in estuaries, *Estuarine, Coastal and Shelf Science, 45*, 113-121.

Curtis, J. H., D. A. Hodell, and M. Brenner (1996), Climate variability on the Yucatan Peninsula (Mexico) during the past 3500 years, and implications for Maya cultural evolution, *Quaternary Research, 46*(1), 37-47.

Cutler, K. B., R. L. Edwards, F. W. Taylor, H. Cheng, J. Adkins, C. D. Gallup, P. M. Cutler, G. S. Burr, and A. L. Bloom (2003), Rapid sea-level fall and deep-ocean temperature change since the last interglacial period, *Earth and Planetary Science Letters*, *206*(3-4), 253-271.

Debret, M., V. Bout-Roumazeilles, F. Grousset, M. Desmet, J. F. McManus, N. Massei, D. Sebag, J.-R. Petit, Y. Copard, and A. Trentesaux (2007), The origin of the 1500-year climate cycles in Holocene North Atlantic records, *Climate of the Past, 3*, 569-575.

Dekens, P. S., D. W. Lea, D. K. Pak, and H. J. Spero (2002), Core top calibration of Mg/Ca in tropical foraminifera: Refining paleotemperature estimation, *Geochemisty, Geophysics, Geosystems, 3*(4), 1022, doi: 10.1029/2001GC000200.

Delworth, T. L. and Mann, M. E. (2000), Observed and simulated multidecadal variability in the Northern Hemisphere, *Climate Dynamics, 16*, 661–676.

deMenocal, P. B., J. Ortiz, T. Guilderson, and M. Sarnthein (2000), Coherent high and low latitude climate variability during the Holocene warm period, *Science*, *288*, 2198-2202.

Dima, M., and G. Lohmann (2007), A hemispheric mechanism for the Atantic multidecadal oscillation, *Journal of Climate, 20*(11), 2706-2719.

Dittert, N, and R. Henrich (2000), Carbonate dissolution in the South Atlantic Ocean: evidence from ultrastructure breakdown in *Globigerinoides bulloides*, *Deep Sea Research, 47*, 603-620.

Edmond, J. M., E. D. Boyle, D. Drummond, B. Grant, and T. Mislick (1978), Desorption of arium in the plume of the Zaire (Congo) River, *Netherlands Journal of Sea Research, 12*(3/4), 324-328.

Edwards, R. L., J. W. Beck, G. S. Burr, D. J. Donahue, J. M. A. Chappell, A. L. Bloom, E. R. M. Druffel, and F. W. Taylor (1993), A large drop in atmospheric C-14/C-12 and reduced metling in the Yougar Dryas, documented with Th-230 ages of corals, *Science*, *260*(5110), 962-968.

Elderfield, H. and G. Ganssen (2000), Past temperatures and d18O of surface ocean water inferred from foraminiferal Mg/Ca ratios, *Nature*, 405, 442-445.

Ellison, C., M. R. Chapman, and I. R. Hall (2006), Surface and Deep Ocean Interactions During the Cold Climate Event 8200 years ago, *Science*, *312*, 1929-1932.

Enfield, D. B., A. M. Mestas-Nunez, and P. J. Trimble (2001), The Atlantic multidecadal oscillation and its relation to rainfall and river flows in the continental U.S., *Geophyscial Research Letters, 28,* 2077-2080.

Fairbanks, R. G. (1989), A 17,000-year glacio-eustatic sea level record: influence of glacial melting rates on the Younger Dryas event and deep-ocean circulation, *Nature, 342*, 637-642.

Fairbanks, R. G., C. D. Charles, and J. D. Wright (1992), Origin of global meltwater pulses, *in Taylor, R.E., ed., Radiocarbon after four decades,* 473-500, Springer Verlag, New York.

Flower, B. P., D. W. Hastings, H. W. Hill, and T. M. Quinn (2004), Phasing of deglacial warming and Laurentide Ice Sheet meltwater in the Gulf of Mexico, *Geology, 32,* 597-600.

Finkel, R. C., and K. Nishiizumi (1997), Beryllium 10 concentrations in the Greenland Ice Sheet Project 2 ice core from 3-40 ka, *Journal of Geophysical Research Oceans, 102*, 26699-26706.

Fisher, T. G., D. G. Smith, and J. T. Andrews (2002), Preboreal oscillation caused by a glacial Lake Agassiz flood, *Quaternary Science Reviews*, *21*(8-9), 873-878.

Giannini, A., J. C. H. Chiang, M. A. Cane, Y. Kushnir, and R. Seager (2001), The ENSO teleconnection to the tropical Atlantic Ocean: Contributions of the remote and local SSTs to rainfall variability in the tropical Americas, *Journal of Climate, 14*, 4530-4544.

Grinsted, A., S. Moore, and S. Jevrejeva (2004), Application of the cross wavelet transform and wavelet coherence to geophysical time series, *Nonlinear Processes in Geophysics, 11*, 561-566.

Hanor, J. S., and L.-H. Chan (1977), Non-conservative behavior of barium during mixing of Mississippi River and Gulf of Mexico waters, *Earth and Planetary Science Letters*, *37*, 242-250.

Hastings, D. W., A. D. Russell, and S. R. Emerson (1998) Foraminiferal magnesium in Globigerinoides sacculifer as a paleotemperature proxy, *Paleoceanography*, 13, 161-169.

Haug, G. K. A., K. A. Hughen, D. M. Sigman, L. C. Peterson, and U. Rohl (2001), Southward migration of the ITCZ through the Holocene, *Science*, *293*, 1304-1308.

Heslop, D., and A. Paul (2011), Can oceanic paleothermometers reconstruct the Atlantic multidecadal oscillation? *Climate of the Past*, *7*, 151-159.

Hodell, D. A., J. H. Curtis, G. A. Jones, A. Higuera-Gundy, M. Brenner, M. W. Binford, and K. T. Dorsey (1991), Reconstruction of Caribbean climate change over the past 10,500 years, *Nature, 352*, 790-793.

Hodell, D. A., M. Brenner, J. H. Curtis and T. Guilderson (2001) Solar forcing of drought frequency in the Maya Lowlands, *Science, 292*(5520), 1367-1370.

Hönisch, B., K. A. Allen, A. D. Russell, S. M. Eggins, J. Bijma, H. J. Spero, D. W. Lea, and J. Yu (2011), Planktonic foraminifers as records of seawater Ba/Ca, *Marine Micropaleontology, 79*, 52-57.

Keigwin, L, (1996), The Little Ice Age and Medieval Warm Period in the Sargasso Sea, *Science*, *274*, 520-523.

Knight, J. R., C. K. Folland, and A. A. Scaife (2006), Climate impacts of the Atlantic Multidecadal Oscillation, *Geophysical Research Letters, 33*(17).

Kukla, G. J., A. C. Clement, M. A. Cane, J. E. Gavin, and S. E. Zebiak (2002), Last interglacial and early interglacial ENSO, *Quaternary Research, 58*, 27-31.

Latif, M., (2000) Tropical Pacific/Atlantic Ocean interactions at multidecadal time scales, Max Planck Institute Rep. 305, Hamburg, Germany, 13 pp.

Lea, D. W., and H. J. Spero (1994), Assessing the reliability of paleochemical tracers: Barium uptake in the shells of planktonic foraminifera, *Paleoceanography 9*(3), 445-452.

Lea, D. W., and P. A. Martin (1996), A raipid mass spectrometric method for the simultaneous analysis of barium, cadmium and strontium in foraminifera shells, *Geochimica et Cosmochimica Acta, 60*, 3143-3149.

Lea, D. W., D. K. Pak, and H. J. Spero (2000), Climate Impact of Late Quaternary Equatorial Pacific Sea Surface Temperature Variations, *Science*, *289*, 1719-1724.

Locarnini, R. A., A. V. Mishonov, J. I. Antonov, T. P. Boyer, and H. E. Garcia (2006), World Ocean Atlas 2005, Volume 1: Temperature. S. Levitus, Ed. NOAA Atlas NESDIS 61, U.S. Government Printing Office, Washington, D.C., 182 pp.

LoDico, J. M., B. P. Flower, and T. M. Quinn (2006), Subcentennial-scale climatic and hydrologic variability in the Gulf of Mexico during the Holocene, *Paleoceanography*, 21, PA3015, doi:10.1029/2005PA001243.

Lorens, R. B., D. F. Williams, and M. L. Bender (1977), Early nonstructural chemical diagenesis of foraminiferal calcite, *Journal of Sedimentary Petrology*, 47, 1602-1609.

Lund, D. C., and W. Curry (2004), Late Holocene variability in Florida Current surface density: Patterns and possible causes, *Paleoceanography*, *19*, doi: 10.1029/2004PA001008.

Lund, D. C., and W. Curry (2006), Florida Current surface temperature and salinity variability during the last millennium, *Paleoceanography*, *21*(2), doi:10.1029/2005PA001218.

Lund, D. C., J. Lynch-Stieglitz, and W. B. Curry (2006), Gulf Stream density structure and transport during the past millennium, *Nature, 444,* 601-604.

Lynch-Stieglitz, J., W. B. Curry, and D. C. Lund (2009), Florida Straits density structure and transport over the last 8000 years, *Paleoceanography*, *24*, 9, doi: 10.1029/2008PA001717.

Mann, M. E., M. A. Cane, S. E. Zebiak, and A. Clement (2005), Volcanic and solar forcing of the tropical Pacific over the past 1000 years, *Journal of Climate, 18*, 447-456.

Marchitto, T. M., R. Muscheler, J. D. Ortiz, J. D. Carriquiry, and A. van Geen (2010), Dynamical response of the tropical Pacific Ocean to solar forcing during the early Holocene, *Science*, 330, 1378-1380.

Mashiotta, T. A., D. W. Lea, and H. J. Spero (1999), Glacial-interglacial changes in Subantarctic sea surface temperature and δ^{18}O-water using foraminiferal Mg, *Earth and Planetary Science Letters*, *170*, 417-432.

Maul, G. A., and F. M. Vukovich (1993), The relationship between variations in the Gulf of Mexico Loop Current and Straits of Florida volume transport, *Journal of Physical Oceanography*, *23*(5), 785-796.

Murphy, S. J., H. E. Hurlburt, and J. J. O'Brian (1999), The connectivity of eddy variability in the Caribbean Sea, the Gulf of Mexico, and the Atlantic Ocean, *Journal of Geophysical Research-Oceans*, *104*(C1), 1431-1453

Nurnberg, D., J. Bijma, and C. Hemleben (1996), Assessing the reliability of magnesium in foraminiferal calcite as a proxy for water mass temperatures*, Geochimica et Cosmochimica Acta, 60*, 803-814.

Oppo, D. W., G. A. Schmidt, A. N. LeGrande (2007), Seawater isotope constraints on tropical hydrology during the Holocene, *Geophysical Research Letters*, *34*(13).

Ortner, P. B., T. N. Lee, P. J. Milne, R. G. Zika, M. E. Clarke, G. P. Podesta, P. K. Swart, P. A. Tester, L. P. Atkinson, and W. R. Johnson (1995), Mississippi River flood waters that reached the Gulf Stream, *Journal of Geophysical Research, 100*, 13595-13601.

Paillard, D., L. Labeyrie, and P. Yiou (1996), Macintosh program performs time-series analysis, *EOS, Transactions of the American Geophysical Union*, *77*(379).

Pena, L. D., E. Calvo, I. Cacho, S. Eggins, and C. Pelejero (2005), Identification and removal of Mn-Mg-rich contaminant phases on foraminiferal tests: Implications for Mg/Ca past temperature reconstructions, *Geochemistry, Geophysics, Geosystems, 6(9)*, Q09P02, doi: 10.1029/2005GC000930.

Peterson, L. C., J. T. Overpeck, N. G. Kipp, and J. Imprie (1991), A high-resolution late Quaternary upwelling record from the anoxic Cariaco Basin, Venezuela, *Paleoceanography, 6*(1), 99-119.

Poore, R. Z., T. M. Quinn, and S. Verardo (2004), Century-scale movement of the Atlantic Intertropical Convergence Zone linked to solar variability, *Geophysical Research Letters*, *31*(12)

Poore, R. Z., H. J. Dowsett, S. Verardo, and T. M. Quinn (2003), Millennial- to century-scale variability in Gulf of Mexico Holocene climate records, *Paleoceanography*, *18*(2), 1048, doi: 10.1029/2002PA000868.

Poveda, G. and O. J. Mesa (1997), Feedbacks between hydrological processes in tropical South America and large-scale ocean–atmospheric phenomena, *Journal of Climate*, *10*, 2690-2702.

Reimer P. J., M. G. L. Baillie, E. Bard, A. Bayliss, J. W. Beck, C. J. H. Bertrand, P. G. Blackwell, C. E. Buck, G. S. Burr, K. B. Cutler, P. E. Damon, R. L. Edwards, R. G. Fairbanks, M. Friedrich, T. P. Guilderson, A. G. Hogg, K. A. Hughen, B. Kromer, G. McCormac, S. Manning, C. B. Ramsey, R. W. Reimer, S. Remmele, J. R. Southon,

M. Stuiver, S. Talamo, F. W. Taylor, J. von der Plicht, and C. E. Weyhenmeyer (2004), IntCal04 terrestrial radiocarbon age calibration, 0-26 cal kyr BP, *Radiocarbon, 46,* 1029-1058.

Richey, J. N., R. Z. Poore, B. P. Flower, T. M. Quinn, and D. J. Hollander (2009), Regionally coherent Little Ice Age cooling in the Atlantic Warm Pool, *Geophysical Research Letters, 36,* doi:10.1029/2009GL040445.

Rosenthal, Y. and E. A. Boyle (1993), Factors controlling the fluoride content of planktonic foraminifera: An evaluation of its paleoceanographic applicability, *Geochemica et Cosmochimica Acta*, 57, 335-346.

Rosenthal, Y., G. P. Lohmann, K. C. Lohmann, and R. M. Sherrell (2000), Incorporation and preservation of Mg in *Globigerinoides sacculifer:* Implications for reconstructing the temperature and $^{18}O/^{16}O$ of seawater, *Paleoceanography,* 15, 135-145.

Roth, S. and J. G. Reijmer (2005), Holocene millennial to centennial carbonate cyclicity recorded in slope sediments of the Great Bahama Bank and its climatic implications, *Sedimentology¸ 52,* 161-181.

Saenger, C., P. Chang, L. Ji, D. W. Oppo, and A. L. Cohen (2009), Tropical Atlantic climate response to low-latitude extratropical sea-surface temperature: A Little Ice Age perspective, *Geophysical Research Letters, 36¸* L11703, doi:10.1029/2009GL038677.

Schmidt, G. A., G. R. Bigg, and E. J., Rohling (1999), Global seawater oxygen 18 database, 1999, available at http://www.giss.nasa.gov/data/o18data/.

Schmidt, M. S., H. J. Spero, and D. W. Lea (2004), Links between salinity variation in the Caribbean and North Atlantic thermohaline circulation, *Nature*, *428*, 160-163.

Schmittner, A., C. Appenzeller, and T. F. Stocker (2000), Enhanced Atlantic freshwater export during El Niño, *Geophysical Research Letters, 27*, 1163–1666.

Schmittner, A., and A. C. Clement (2002), Sensitivity of the thermohaline circulation to tropical and high latitude freshwater forcing during the last glacial-interglacial cycle, *Paleoceanography, 17*, 1017, doi: 10.1029/2000PA000591.

Schmitz, W. J., and P. Richardson (1991), On the sources of the Florida Current, *Deep Sea Research, 38,* 379-409.

Siddall, M., E. Bard, E. J. Rohling, and C. Hemleben (2003), Sea-level fluctuations during the last glacial cycle, *Nature, 423,* 853-858).

Spero, H. J., K. M. Mielke, E. M. Kalve, D. W. Lea, and D. K. Pak (2003), Multispecies approach to reconstructing eastern equatorial Pacific thermocline hydrography during the past 360 kyr, *Paleoceanography*, *18*(1), doi:10.1029/2002PA000814.

Stuiver, M., T. F. Braziunas, B. Becker, and B. Kromer (1991), Climatic, solar, oceanic, and geomagnetic influences on late-glacial and Holocene atmospheric $^{14}C/^{12}C$ change, *Quaternary Research, 35*, 1-24.

Stuiver, M., P. J. Reimer, and R. Reimer (2005), CALIB 6.0. [WWW program and documentation].

Turekian, K. K., and D. G. Johnson (1966), The barium distribution in sea water, *Geochemica et Cosmochimica Acta, 30*, 1153+1174.

van Raden, U. J., J. Groeneveld, M. Raitzsch, and M. Kucera (2011), Mg/Ca in the planktonic foraminifera *Globorotalia inflata* and *Globigrinoides bulloides* from Western Mediterranean plankton tow and core top samples, *Marine Micropaleontology*, (78), 101-112.

Vonmoos, M., J. Beer, and R. Muscheler (2006), Large variations in Holocene solar activity: Constraints from Be-10 in the Greenland Ice Core Project ice core, *Journal of Geophysical Research Space Physics, 111,* A10105.

Waelbroeck, C., A. Paul, M. Kucera, A. Rosell-Melee, M. Weinelt, R. Schneider, A. C. Mix, A. Abelmann, L. Armand, E. Bard, S. Barker, T. T. Barrows, H. Benway, I. Cacho, M. T. Chen, E. Cortijo, X. Crosta, A. de Vernal, T. Dokken, J. Duprat, H. Elderfield, F. Eynaud, R. Gersonde, A. Hayes, M. Henry, C. Hillaire-Marcel, C. C. Huang, E. Jansen, S. Juggins, N. Kallel, T. Kiefer, M. Kienast, L. Labeyrie, H. Leclaire, L. Londeix, S. Mangin, J. Matthiessen, F. Marret, M. Meland, A. E. Morey, S. Mulitza, U. Pflaumann, N. G. Pisias, T. Radi, A. Rochon, E. J. Rohling, L. Sbaffi, C. Schafer-Neth, S. Solignac, H. Spero, K. Tachikawa, J. L. Turon, and M. P. Members (2009), Constraints on the magnitude and patterns of ocean cooling at the Last Glacial Maximum, *Nature Geoscience*, 2, 127-132.

Wagner, G., J. Masarik, J. Beer, S. Baumgartner, D. Imboden, P. W. Kubik, H. A. Synal, and M. Suter (2000), Reconstruction of the geomagnetic field between 20 and 60 kyr BP from cosmogenic radionuclides in the GRIP ice core, *Nuclear Instruments and Methods in Physics Research Section B: Beam Interactions with Materials and Atoms, 172*, 597-604.

Walker, N. D., W. J. Wiseman, Jr., L. J. Rouse, Jr., and A. Babin (2005), Effects of river discharge, wind stress, and slope eddies on circulation and the satellite-observed

structure of the Mississippi River plume, *Journal of Coastal Research*, *21*(6), 1228-1244.

Wang, Y., H. Cheng, R. L. Edwards, Y. He, X. Kong, Z. An, J. Wu, M. J. Kelly, C. A. Dykoski, and X. Li (2005), The Holocene Asian monsoon: Links to solar changes in North Atlantic climate, *Science 6*, 854-857.

APPENDIX A FIGURES

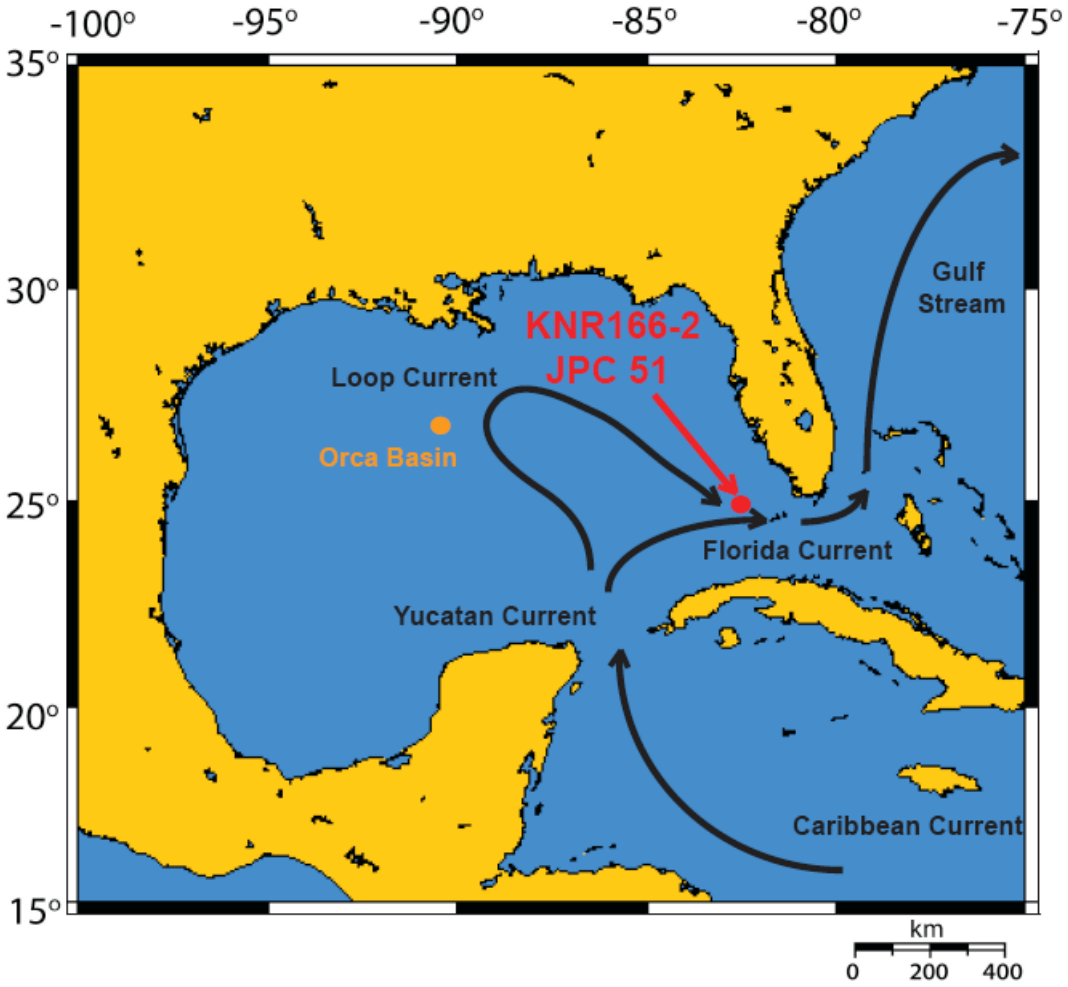

Figure 1 Site Location. The location of the core used in this study, KNR166-2 JPC 51 on the northern margin of the Florida Straits. Also noted is the position of the Orca Basin in the northern Gulf of Mexico (map generated using OMC *www.aquarius.geomar.de/*, 2009).

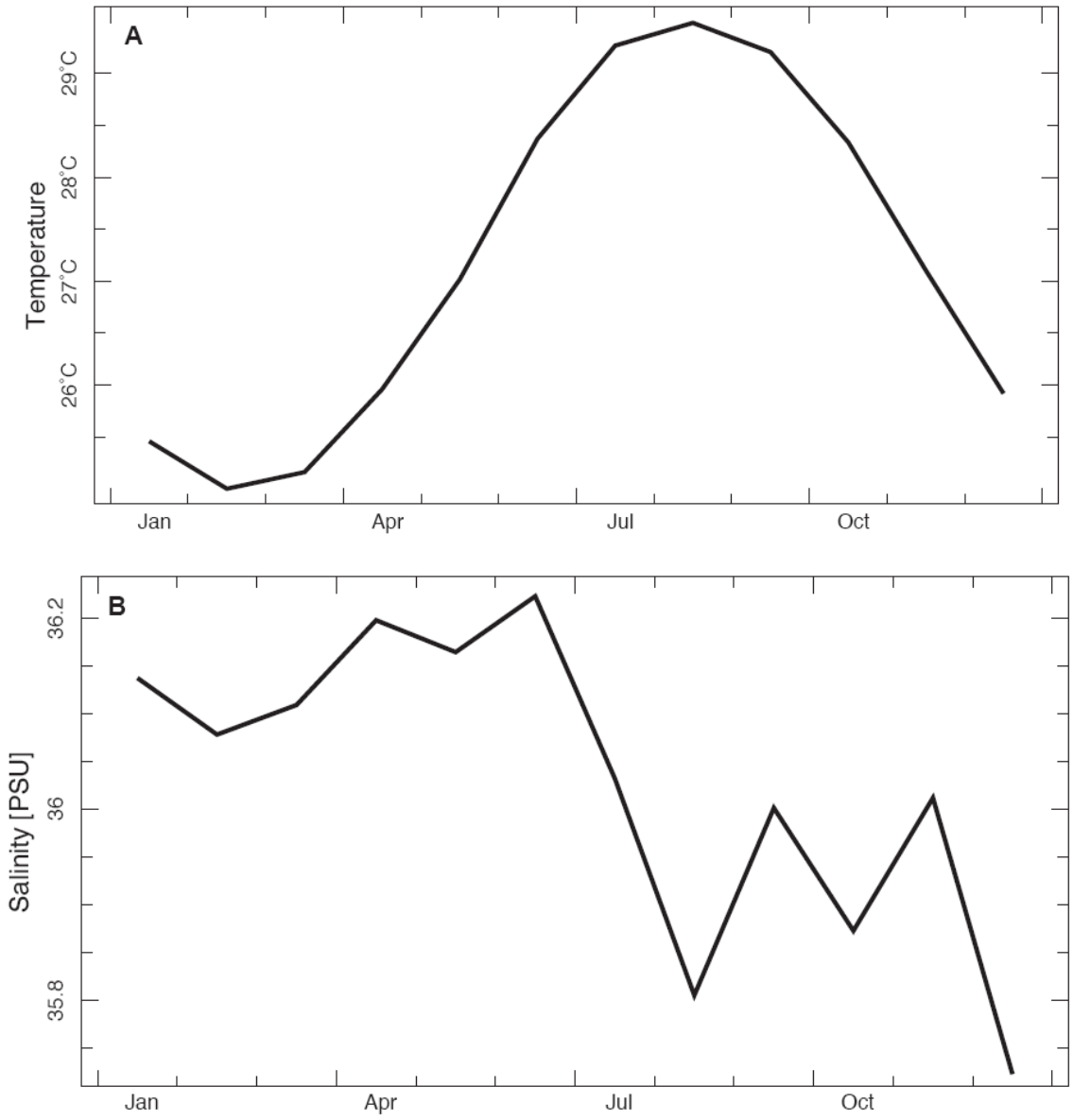

Figure 2 Modern SST and SSS. (A) Modern annual SST [*Locarnini et al.,* 2006] and (B) SSS [*Antonov et al.,* 2006] in the Florida Straits at the site location of JPC-51.

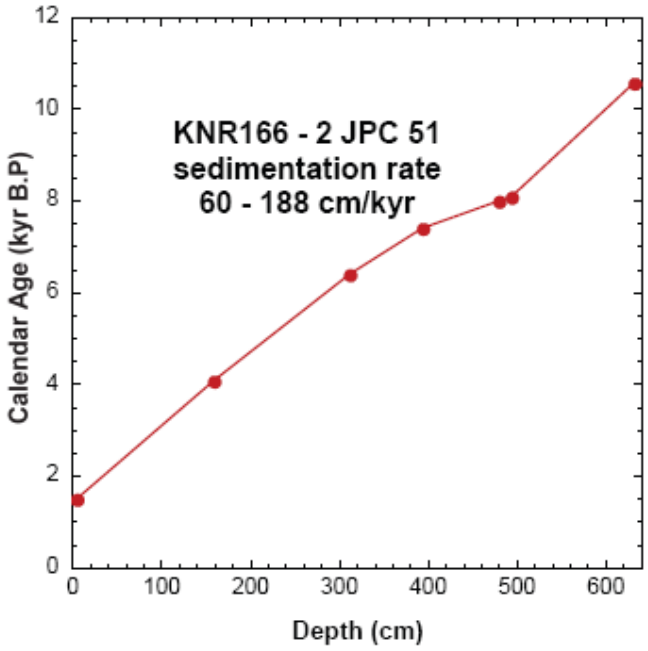

Figure 3 Age Model. Calendar age vs. core depth for JPC 51 based on ^{14}C dates from mixed samples of *G. ruber* and *G. sacculifer* shell material. Radiocarbon years were calibrated to calendar years using CALIB 6.0 [*Stuiver et. al*, 2005].

A.

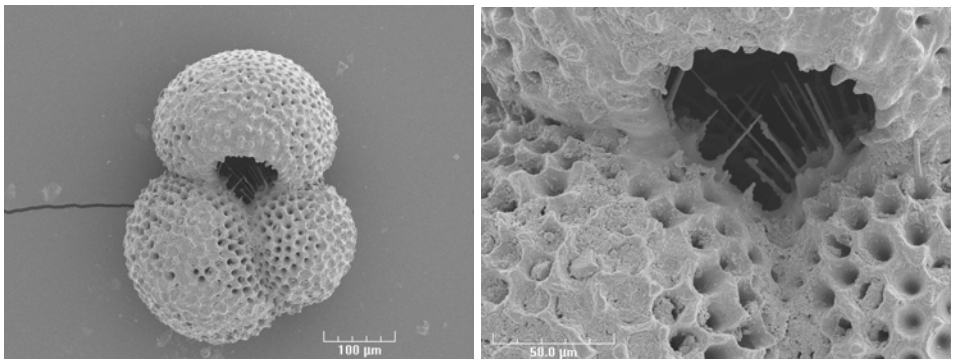

B.

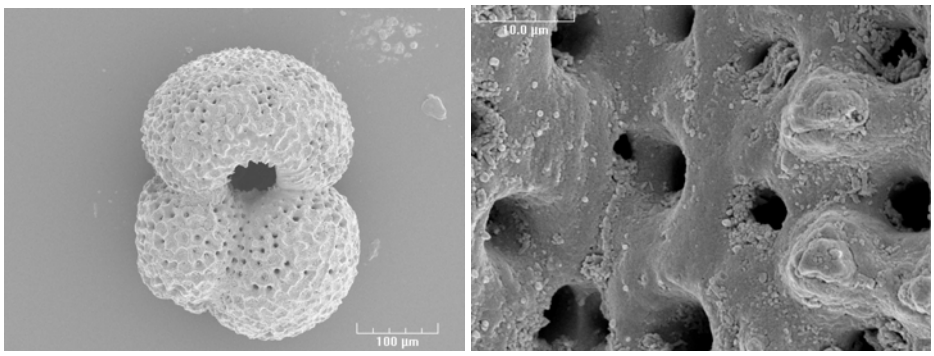

Figure 4 SEM Photographs. SEM photos of *G. ruber* shells from an interval characterized by a high Mg/Ca ratio (A) and low Mg/Ca ratio (B). Note the unaltered appearance of the shell surface and the presence of only clays filling the pores (removed in the cleaning process). There is no evidence of crystal growth or dissolution pits, suggesting that diagenetic overprinting is unlikely (images courtesy of Bridget Wade).

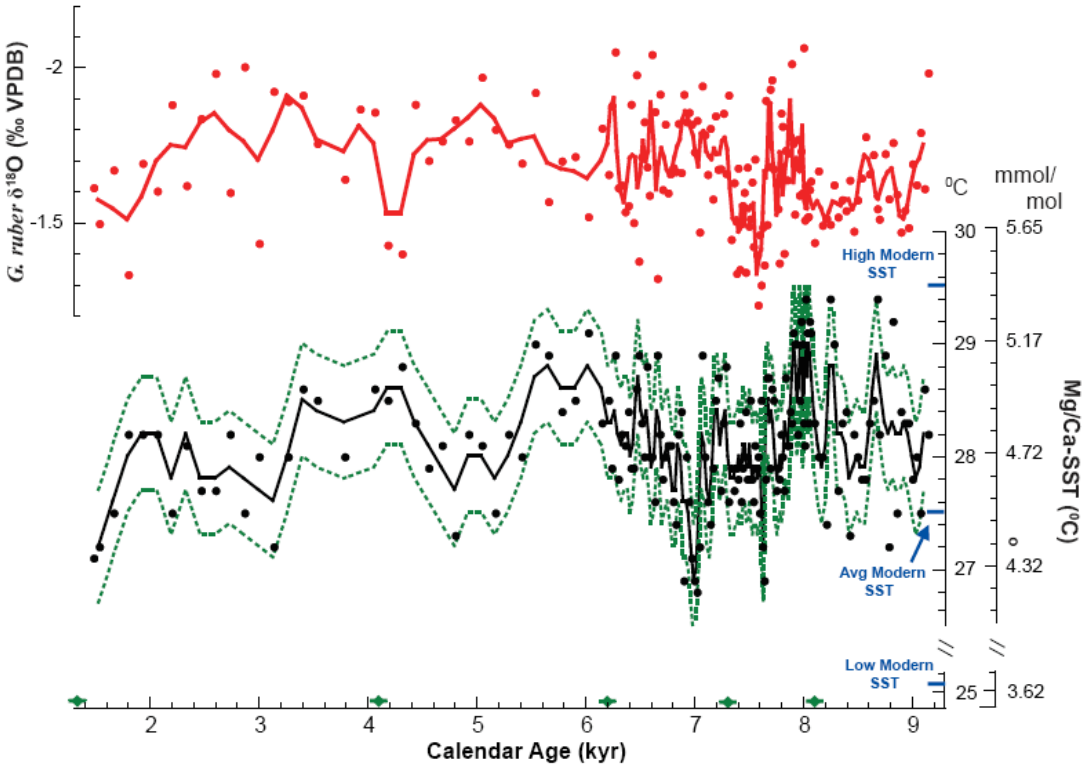

Figure 5 *G. ruber* $\delta^{18}O$ and Mg/Ca-SST. $\delta^{18}O$ values in *G. ruber* collected from the Florida Straits (JPC 51) (red line – 3-point smoothed) and corresponding unsmoothed values. Mg/Ca-SSTs (black line – 3-point smoothed) and corresponding actual values with a Mg/Ca (mmol/mol) scale from JPC 51 calculated using the general planktonic relationship from *Anand et al.* [2003]: Mg/Ca = 0.38 exp 0.09(SST). The optimistic 1σ error of ±0.5°C is shown with the green dashed line around the smoothed SST record. In blue along the SST axis are the high and low annual SST values for the Florida Straits and the average annual SST. Green diamonds on the x-axis indicate intervals with radiocarbon dates and their associated error.

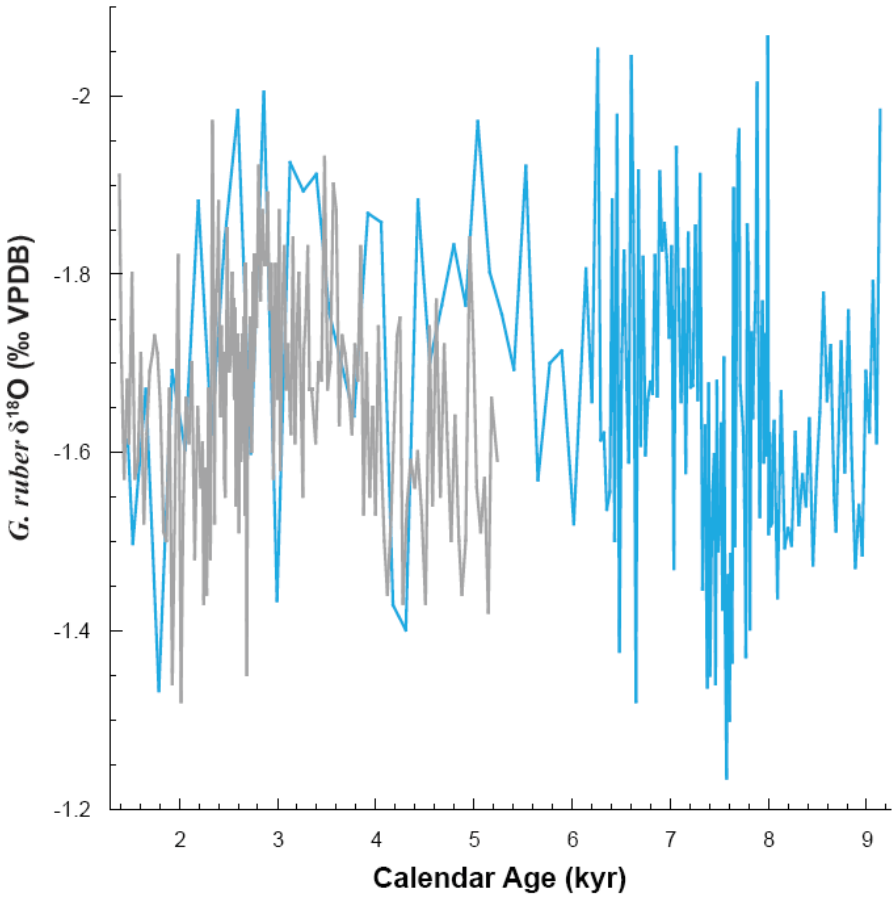

Figure 6 Florida Straits $\delta^{18}O_{calcite}$ Comparison. Comparison of raw $\delta^{18}O_{calcite}$ records between JPC 51 (blue line, this study) and 79 GGC (grey line, [*Lund and Curry*, 2004]). Note the similarities between the oscillations in each of the two records throughout the Holocene. The cycles found in the early Holocene have a similar magnitude and period to those found by *Lund and Curry* [2004] in the late Holocene.

Figure 7 $\delta^{18}O_{SW}$, $\delta^{18}O_{IVF\text{-}SW}$ and Ba/Ca Comparison. (**A**) Calculated $\delta^{18}O_{SW}$ values from JPC 51 (green circles with weighted 3-point smooth) using the *Bemis et al.* [1998] relationship: (T°C) = 16.5 - 4.80 ($\delta^{18}O_{calcite}$ - $\delta^{18}O_{SW}$) and the Mg/Ca-SST relationship from *Anand et al.* [2003]. (**B**) Global $\delta^{18}O_{SW}$ change due to continental ice volume variability (blue) from a compilation of sea level records for the last 10 kyr [*Bard et al.,* 1990; *Cutler et al.* 2003; *Edwards et al.,* 1993] and the relationship that a one meter increase in sea level change equates to a change of –0.008‰ in global $\delta^{18}O_{sw}$ values [*Siddall et al.,* 2003]. (**C**) Calculated ice volume free $\delta^{18}O_{SW}$ ($\delta^{18}O_{IVF\text{-}SW}$) (orange circles with weighted 3-point smooth) calculated by correcting for global $\delta^{18}O_{SW}$ change due to continental ice volume variability. (**D**) Foraminiferal Ba/Ca ratios in *G. ruber* (purple) from JPC 51.

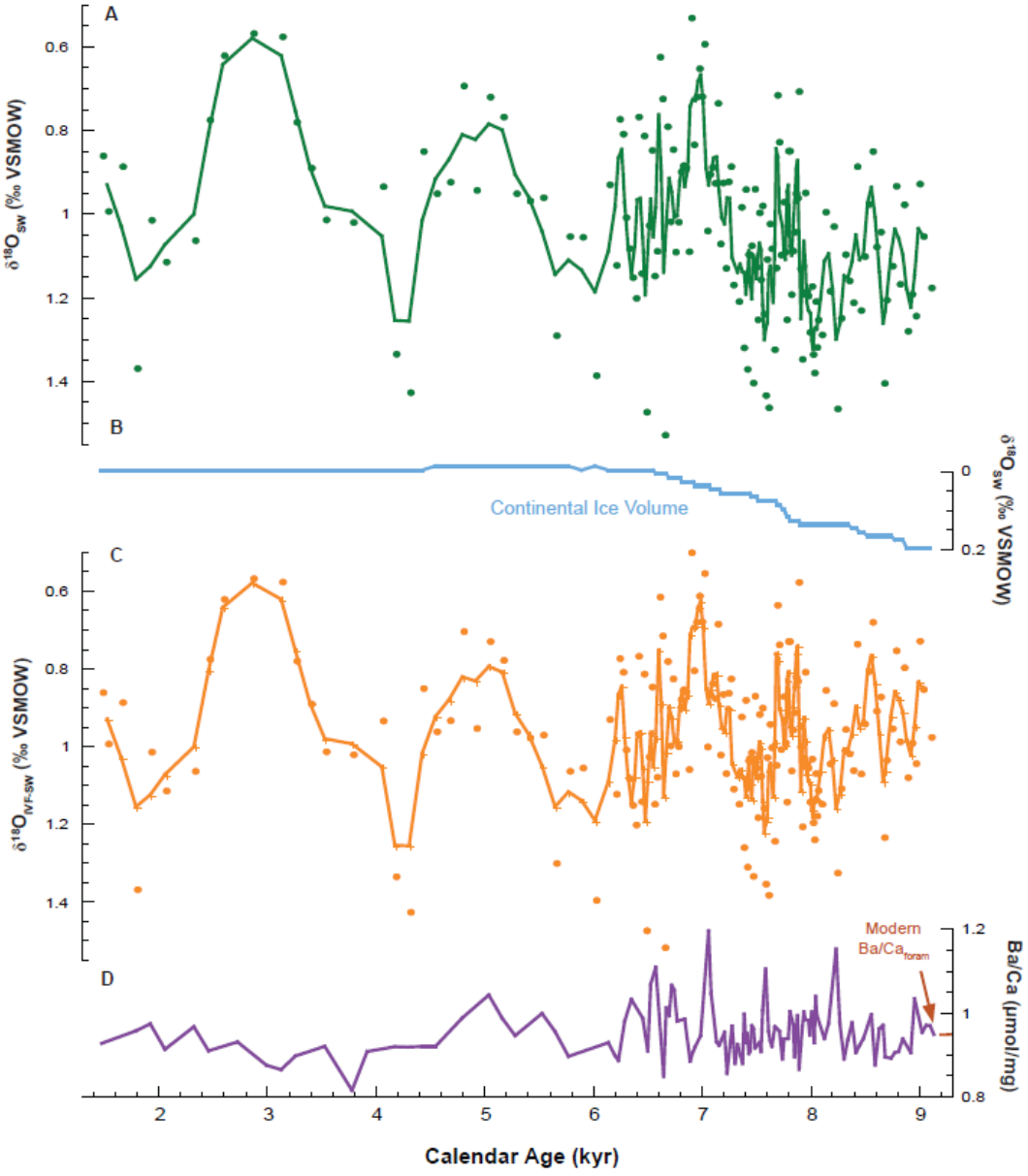
A
B
C
D
$\delta^{18}O_{sw}$ (‰ VSMOW)
Continental Ice Volume
$\delta^{18}O_{IVF-SW}$ (‰ VSMOW)
Modern
Ba/Ca_{foram}
Ba/Ca (µmol/mg)
Calendar Age (kyr)

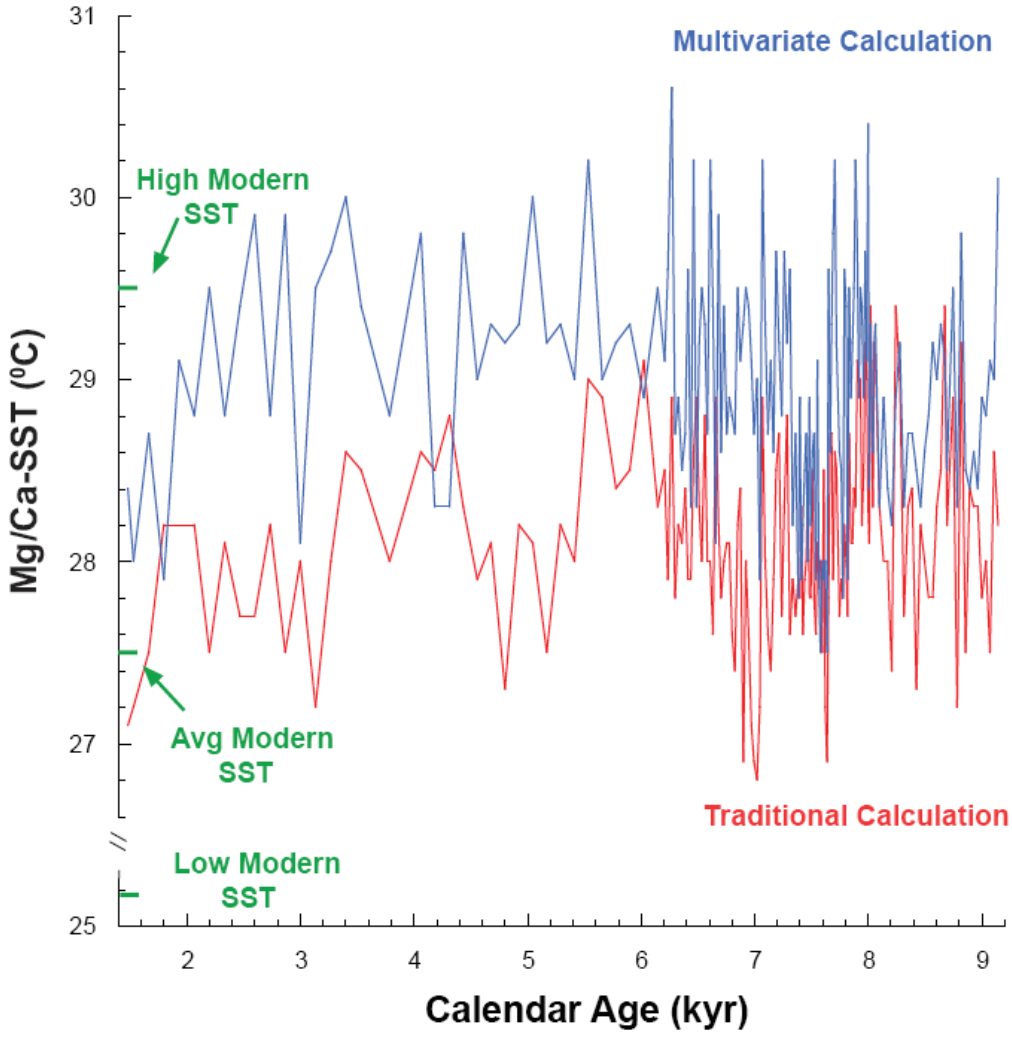

Figure 8 Multivariate and Traditional Mg/Ca-SST Comparison. Comparison of the Mg/Ca-SST reconstructions calculated using the traditional relationship in *Anand et al.* [2003] (red) and the multivariate equations from *Arbuszewski et al.* [2010] (blue). Using the multivariate equations results in SSTs that are, on average, 0.8°C warmer and considerably warmer then the modern average of 27.5°C. The upper and lower bounds, as well as average modern SSTs are identified in green along the y-axis.

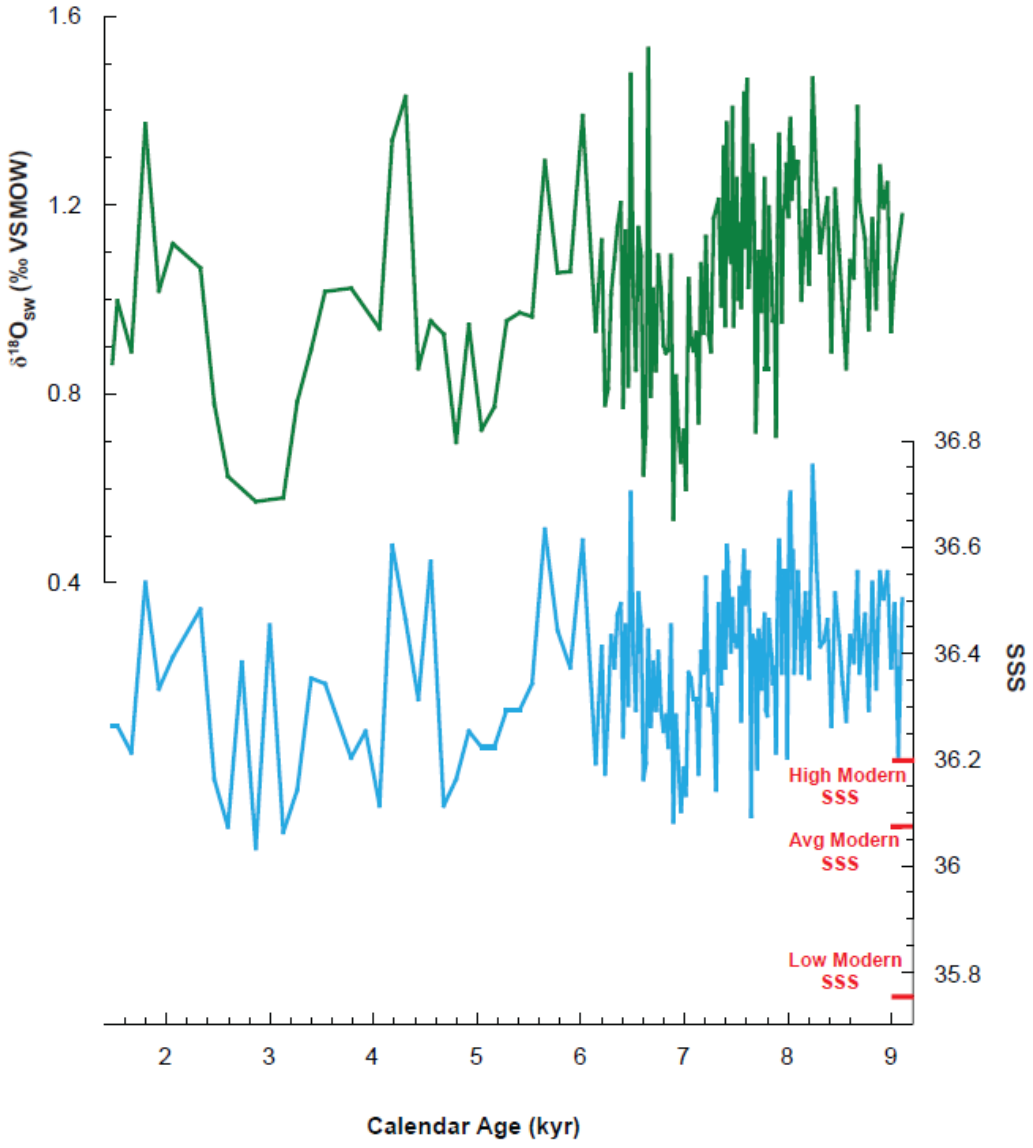

Figure 9 $\delta^{18}O_{SW}$ and Mulitvariate SSS Comparison. A comparison between the methods used in this paper to calculate $\delta^{18}O_{sw,}$ in red and calculating SSS using the multivariate relationship, in blue [*Arbuszewski et al.,* 2010]. Notice the timing of the increased salinity change is the same, and only the magnitude is reduced using the multivariate equation.

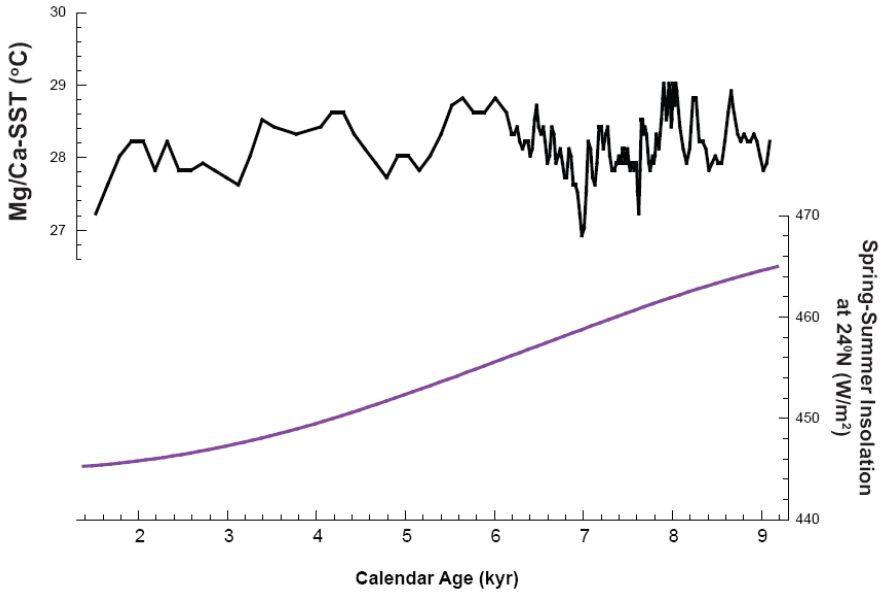

Figure 10 Mg/Ca-SST and Spring-Summer Insolation Comparison. Mg/Ca-SST of JPC 51 compared to record of spring-summer insolation at 24°N through the Holocene. Note the subtle decrease in SST over the Holocene that may reflect lower spring-summer insolation.

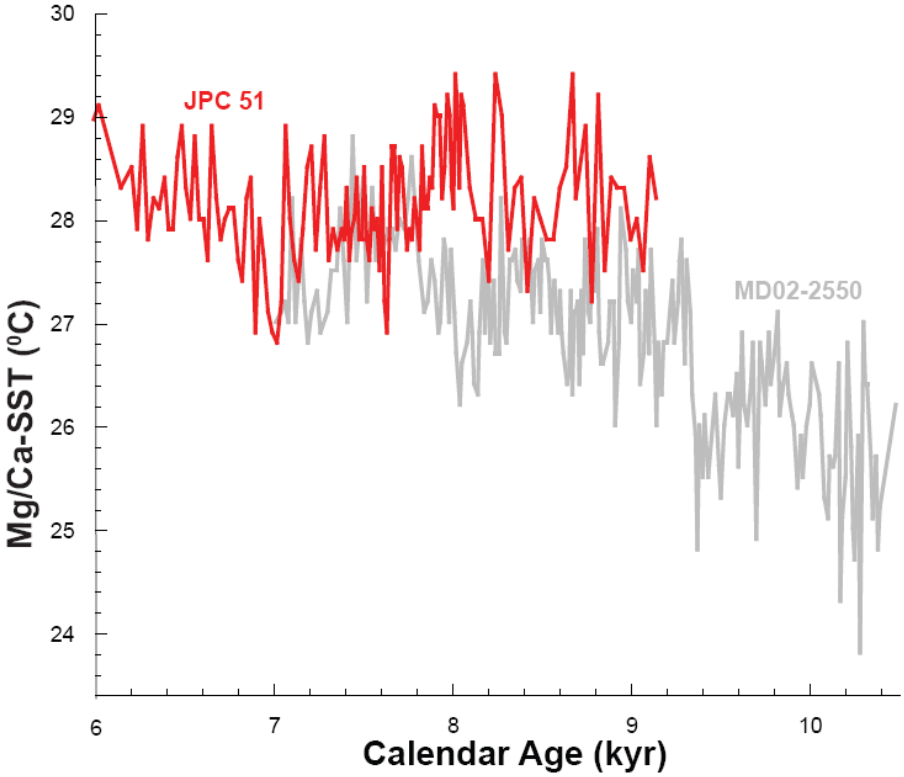

Figure 11 Orca Basin and Florida Straits SST Comparison. The Mg/Ca-SST derived records for both the Florida Straits (JPC 51 in red) and the Orca Basin (MD02-2550 in gray) calculated using the Mg/Ca-SST relationship in *Anand et al.* [2003] and the $\delta^{18}O_{Calcite}$:SST relationship in *Bemis et al.* [1998].

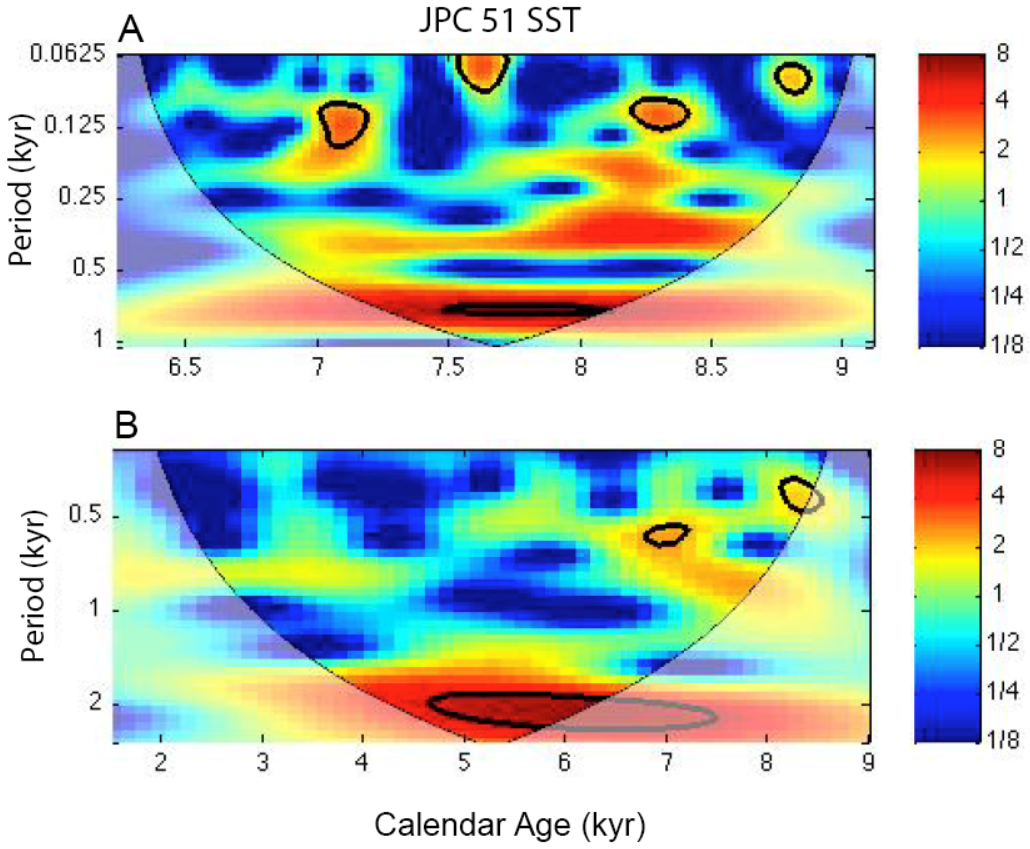

Figure 12 SST Wavelet Analysis. (**A**) Wavelet analysis of the high-resolution JPC 51 SST record during the early Holocene (9.1 – 6.2 kyr) showing spectral power at 70, 125 and 800 year periods above the 95% confidence level. (**B**) Wavelet analysis of the lower-resolution Holocene record from 1.5 – 9.1 kyr showing spectral power at 600 and 2,000 year periods above the 95% confidence interval envelope. On the wavelet power spectrums, red corresponds to high spectral power while blue corresponds to low spectral energy power.

Figure 13 Ba/Ca, $\delta^{18}O_{IVF\text{-}SW}$, and Insolation Comparison. (A) Foraminiferal Ba/Ca ratios in *G. ruber* from JPC 51. **(B)** Comparison of the ice volume corrected $\delta^{18}O_{SW}$ records from the Florida Straits during the late Holocene, 79 GGC in red [*Lund and* Curry, 2004] and during the early Holocene from the Florida Straits and Orca Basin, JPC 51 in red and MD02-2550, in gray [*LoDico et al.,* 2006], respectively. **(C)** Record of titanium percentage in Cariaco Basin, ODP Site 1002 [*Haug et al.,* 2001] and **(D**) spring and summer insolation values for 24°N (blue line), calculated using data from *Paillard et al.* [1996]. The Cariaco Basin titanium record is thought to indicate precipitation variability over South America and the Caribbean associated with north-south shifts in the ITCZ. The % Ti values are high during the early Holocene, suggesting northward migration of the ITCZ and wetter conditions over northern Venezuela [*Haug et al.,* 2001]. Conversely, a drier circum-Caribbean climate and a southward shift in the ITCZ results in reduced % Ti values.

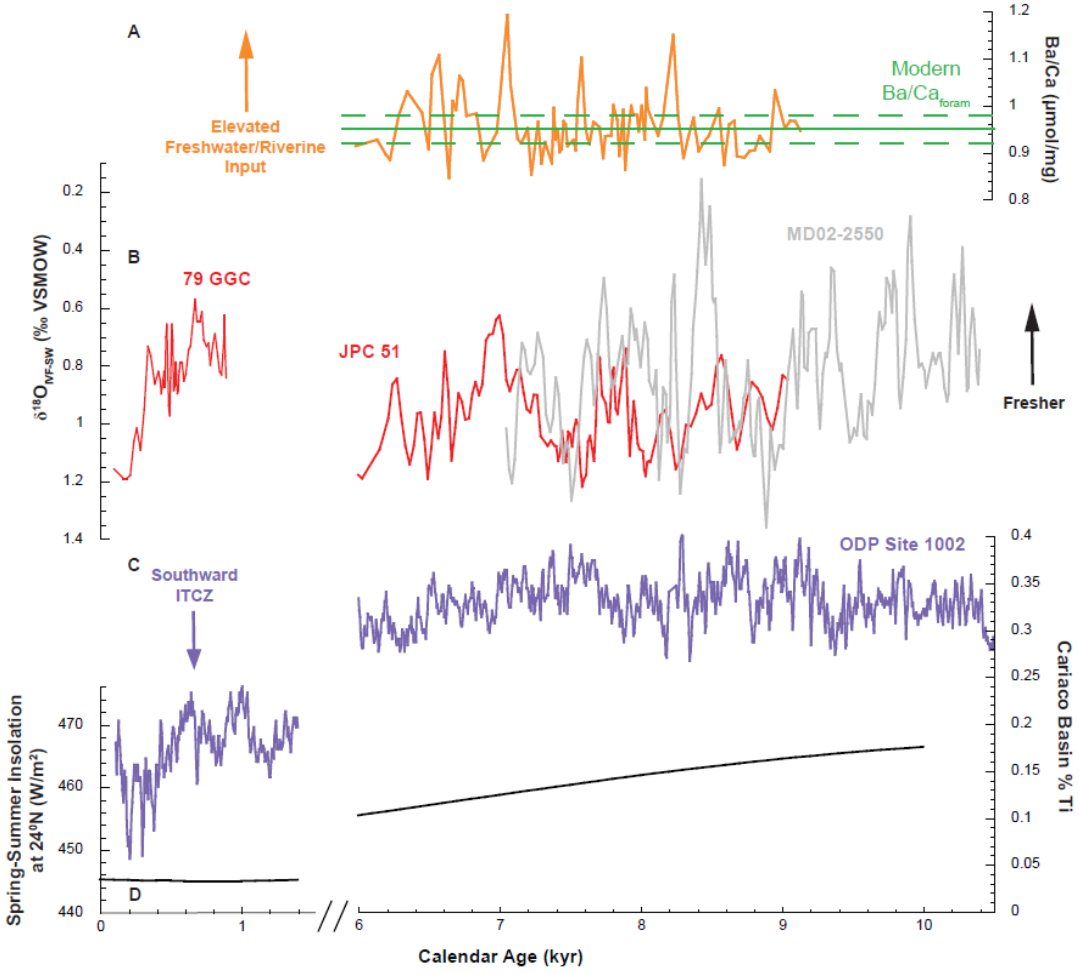
A
Elevated
Freshwater/Riverine
Input
Modern
Ba/Ca foram
Ba/Ca (µmol/mg)
1.2
1.1
1
0.9
0.8
B
79 GGC
JPC 51
MD02-2550
Fresher
δ18OMF-SW (‰ VSMOW)
0.2
0.4
0.6
0.8
1
1.2
1.4
C
Southward
ITCZ
ODP Site 1002
Cariaco Basin % Ti
0.4
0.35
0.3
0.25
0.2
0.15
0.1
0.05
0
Spring-Summer Insolation
at 24°N (W/m²)
470
460
450
440
D
0
1
6
7
8
9
10
Calendar Age (kyr)

Figure 14 Global Teleconnection Comparison. **(A)** 250-year smoothing of early Holocene $\delta^{18}O_{SW}$ from the Florida Straits, JPC 51. **(B)** Record of foraminiferal Mg/Ca-SST from the Soledad Basin, off Baja California Sur, Mexico, during the early Holocene [*Marchitto et al.,* 2010]. **(C)** Stalagmite $\delta^{18}O$ from the Dongge Cave, southern China, which is associated with the strength of the Asian monsoon [*Yang et al.* 2005]. **(D)** Stacked ice-rafted debris record from the North Atlantic [*Bond et al.,* 2001] indicating times of cooler North Atlantic climate when IRD increases **(E)** Global ^{14}C production rates from tree ring records [*Reimer et al.*, 2004] and **(F)** ^{10}Be flux from GRIP-GISP2 [*Finkel and Nishiizumi*, 1997; and *Vonmoos et al.*, 2006], both proxies for solar activity. ^{14}C and ^{10}Be are the product of cosmic rays in the atmosphere, the more active the sun is, the greater the earth is bombarded with these rays, thereby increasing ^{14}C and ^{10}Be ratios in proxy records. Here we can see the connection between development of reduced solar output, El Niño events in the eastern equatorial Pacific and fresher conditions in the North Atlantic and saltier conditions in the Florida Straits, suggesting that changes in solar output had a significant impact on the global hydrologic cycle. Also indicated with the shaded gray bar is the 8.2 kyr event. Note the 8.2 kyr event occurs at a time of increasing solar activity, but that SSS remained elevated in the Florida Straits and SST's in the EEP remain warm. This suggests the cool conditions in the North Atlantic caused by freshwater forcing prevented the tropics from responding to the increase in solar activity at this time.

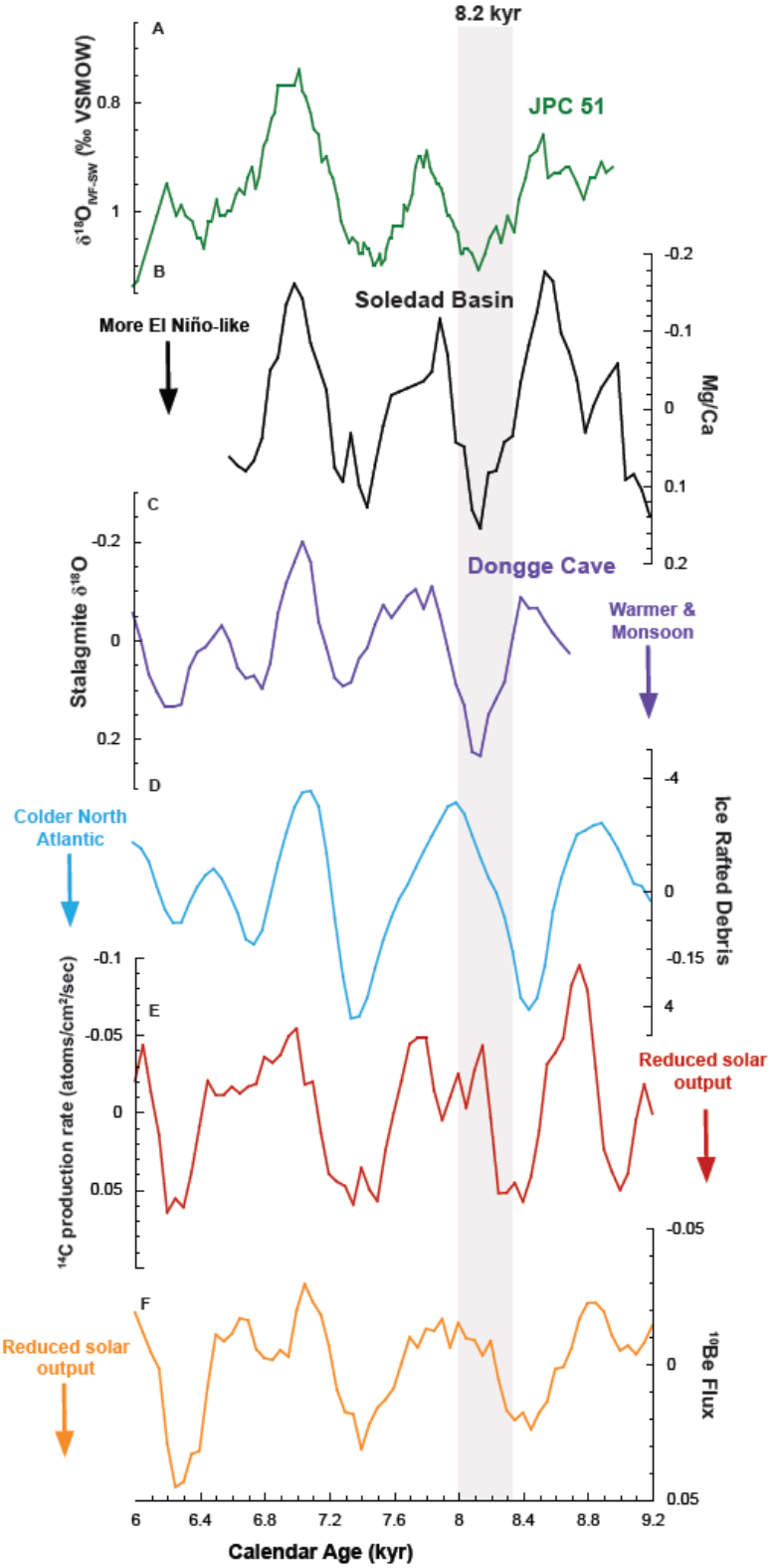
8.2 kyr
A
JPC 51
$\delta^{18}O_{IWF-SW}$ (‰ VSMOW)
0.8
1
B
Soledad Basin
More El Niño-like
-0.2
-0.1
0
0.1
0.2
Mg/Ca
C
Dongge Cave
Stalagmite $\delta^{18}O$
-0.2
0
0.2
Warmer & Monsoon
D
Colder North Atlantic
-4
0
-0.15
4
Ice Rafted Debris
^{14}C production rate (atoms/cm^2/sec)
-0.1
-0.05
0
0.05
E
Reduced solar output
F
Reduced solar output
-0.05
0
0.05
^{10}Be Flux
6
6.4
6.8
7.2
7.6
8
8.4
8.8
9.2
Calendar Age (kyr)

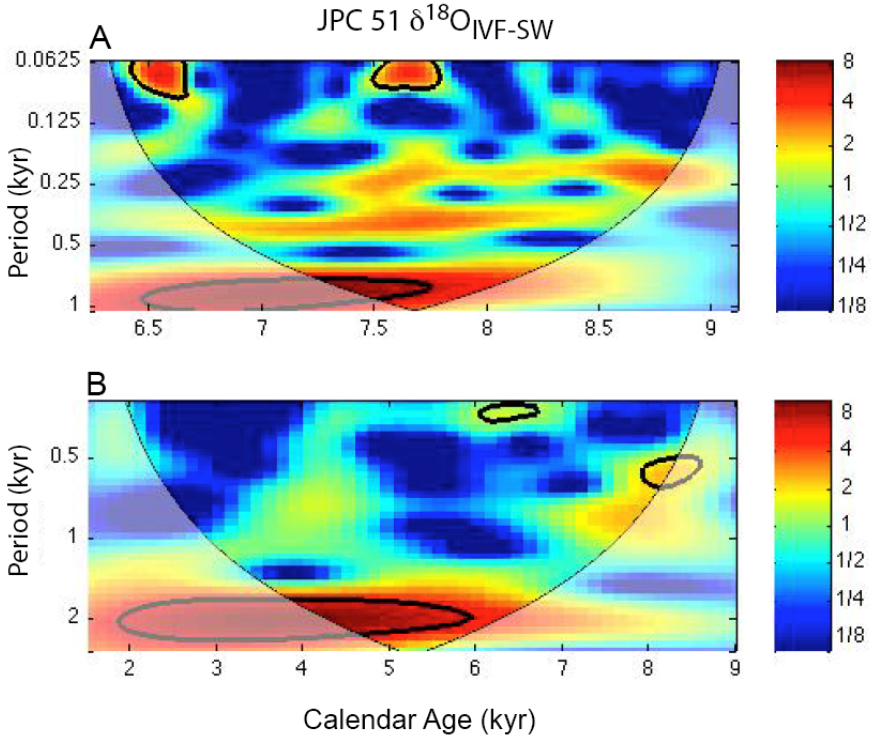

Figure 15 $\delta^{18}O_{IVF\text{-}SW}$ Wavelet Analysis. (**A**) Wavelet analysis of normalized $\delta^{18}O_{IVF\text{-}SW}$ during the early Holocene from 9.1 to 6.2 kyr showing spectral power at periods of 800 and 70 years, both above the 95% confidence level. (**B**) Wavelet analysis of the lower resolution $\delta^{18}O_{IVF\text{-}SW}$ record across the entire Holocene showing spectral power at a periods 2000 years, all above the 95% confidence level.

Figure 16 $\delta^{18}O_{IVF\text{-}SW}$ Spectral Analysis. Spectral analysis of $\delta^{18}O_{IVF\text{-}SW}$ oscillations in JPC-51 shows peaks at 70, 200 and 600-year periods. Spectral power at the 200-year period is common in proxies forced by solar variability, reflecting the ~200 year Suess or Devries solar cycle [*Stuiver and Braziunas*, 1991], further evidence for the dominate influence of solar variability on the JPC 51 surface salinity proxy record..

Figure 17 $\delta^{18}O_{IVF-SW}$ Cross Wavelet Transforms. (A) Cross wavelet transforms between the JPC 51 $\delta^{18}O_{IVF-SW}$ record and the ^{14}C and **(B)** ^{10}Be solar proxies. Arrows indicate the phase angle between the records: horizontal arrow pointing to the right is in phase, pointing to the left is out of phase, and pointing down is 90º out of phase. The strongest common power in both cross wavelet transforms is at periods of about 0.8 to 1 kyr. At these periods, there is a 0º phase angle and the common power is above the 95% confidence interval. The JPC 51 $\delta^{18}O_{IVF-SW}$ record and the ^{14}C production record share common power above the 95 % confidence interval at periods of 200 and 70 years. The cross wavelet transform with the ^{10}Be record also shows significant common power at the 70 year period extending forward of ~8.0 kyr as well as shared common power at the 200 year period before ~8.1 kyr (although the power at this period is below the 95% confidence level). Spectral power at the 200 year period is common in proxies forced by solar variability, reflecting the ~200 year Suess or Devries solar cycle [*Stuiver and Braziunas*, 1991] and spectral power at the 70 year period suggests a possible link to the internally forced Atlantic multidecadal oscillation (AMO) (30-80 year period) [*Dima and Lohmann*, 2007].

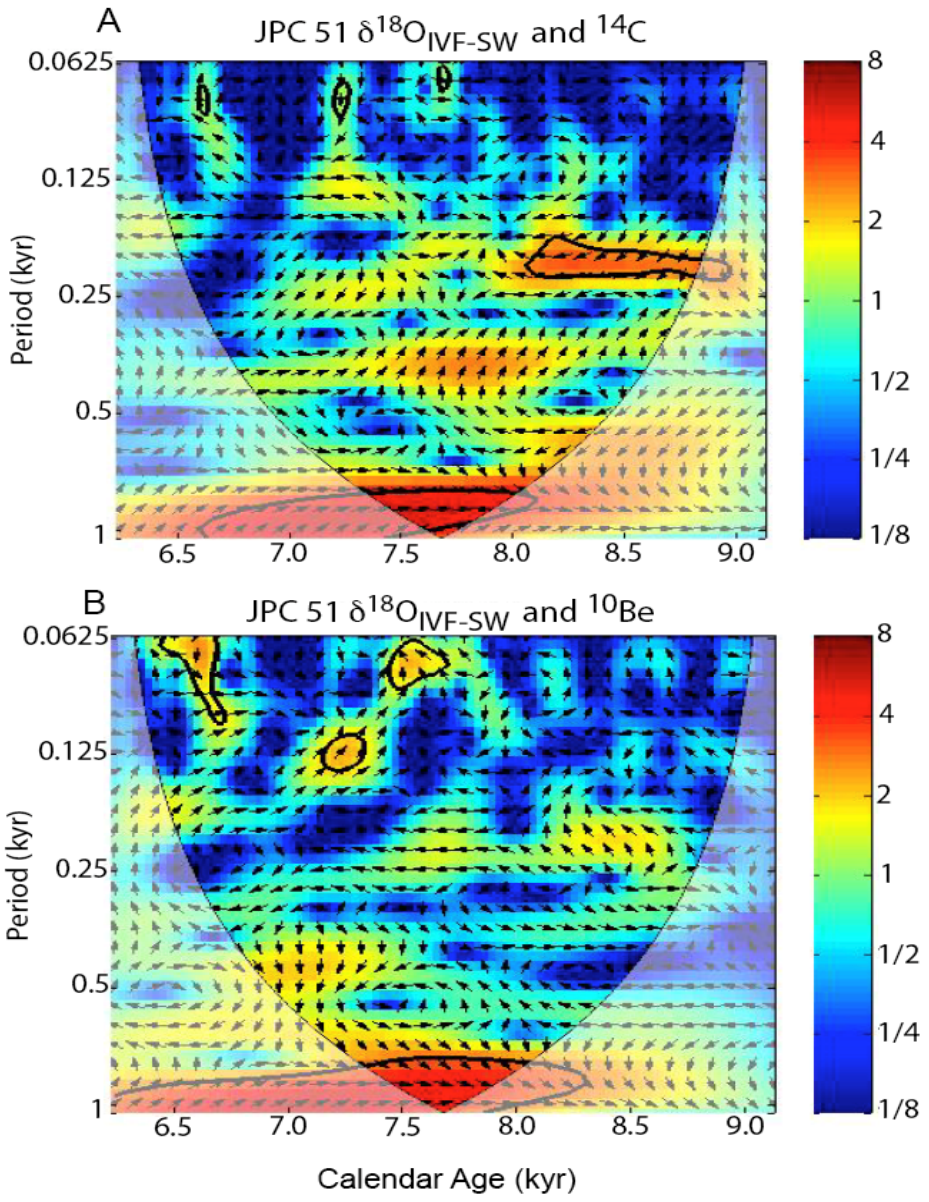
A
JPC 51 δ18OIVF-SW and 14C
0.0625
0.125
0.25
0.5
1
Period (kyr)
6.5
7.0
7.5
8.0
8.5
9.0
8
4
2
1
1/2
1/4
1/8
B
JPC 51 δ18OIVF-SW and 10Be
0.0625
0.125
0.25
0.5
1
Period (kyr)
6.5
7.0
7.5
8.0
8.5
9.0
Calendar Age (kyr)
8
4
2
1
1/2
1/4
1/8

APPENDIX B TABLES

Table 1. AMS ^{14}C and Calendar Ages

Core	Depth, cm	CAMS #	^{14}C Age	Error, yrs	Calendar age, kyr B.P.	Error, yrs
JPC 51	5.25	40017	1940	40	1.49	110
JPC 51	159.25	49009	4040	45	4.07	146
JPC 51	312.25	40018	5970	60	6.40	131
JPC 51	394.5	76076	6880	40	7.39	87
JPC 51	480.25	40019	7520	70	7.99	152
JPC 51	494.5	76077	7610	35	8.07	90
JPC 51	632.25	40020	9690	75	10.56	194

Table 2. JPC 51 $\delta^{18}O_{IVF\text{-}SW}$ Correlations

JPC 51 $\delta^{18}O_{IVF\text{-}SW}$	**Soledad Basin Mg/Ca**	**Dongge Cave $\delta^{18}O$**	**IRD with 100 yr lag**	**^{14}C (solar proxy)**	**^{10}Be (solar proxy)**
r =	0.74	0.58	0.44	0.38	0.41
p-value	1.68E-09	1.25E-05	0.0009	0.0041	0.0019

VITA

Name:	William Adam Weinlein
Address:	Southwest Geoscience 11381 Meadowglen Lane, Suite G Houston, TX 77063
Email Address:	wmaweinlein@gmail.com
Education:	B. S., Geology and Marine Science, Rutgers, the State University of New Jersey, 2008 M. S., Oceanography, Texas A&M University, 2011